IN PASS CALIBRATION DURING LASER RANGING OPERATION

P. Kloeckler, I. Bauersima
Astronomisches Institut
Sidlerstrasse 5 CH 3012 Bern

Telephone 31 65 85 91
Telex 32320

ABSTRACT

In order to avoid atmospheric refraction problems encountered with external targets, an internal calibration path was included in the Zimmerwald LRS. Light is picked up in front of the transmitting telescope, attenuated by diffuse reflection via two spheres plus a variable density filter, and fiber coupled to the receiver photomultiplier. The same discriminator/time digitizer - channel is used both for ranging and calibration. Selection of one calibration shot in n rangings is by range gate setting only. Pulse strength is also recorded. Thus a comprehensive record of internal range bias and its temporal variation is kept, and residual discriminator time walk can be corrected for.

1. CONCEPT

The convenience of in-pass, or feedback, calibration has been noted before (Silverberg, 1982). In fact, there is no compelling reason for external calibrations at all, save for residual range bias tests with terrestrial surveying methods.
In contrast to the TLRS method, we strictly wanted to use the same path and vernier time unit (TDC) both for calibration and ranging. Since the load on our minicomputer is heavy, we could not expect to read out the TDC during the time-of-flight to lower satellites. Thus, every n-th shot has to be sacrified for calibration. This is no great loss because the return probability is not much modified by this in the few photoelectron mode. The selection of ranging/calibration is then by range gate only. Pulse charge is also recorded.

2. PRESENT STATUS

Light is picked up in front of the transmitting telescope, attenuated by diffuse reflection via two spheres plus a variable density filter, and coupled into the receiving optics via light fibre. A chopper-wheel in front of the optics gates out atmospheric backscatter. This serves to reducing unnecessary loading of the photomultiplier as well as permitting pulse strenght recording with a gate time not compatible with spurious returns shortly after the calibration pulse*) (Fig. 1).
Two light paths can be realized for calibration:
a) via light fibre and b) via diffuse reflection onto the primary mirror (used for calibration of the light fibre delay).
The ranging electronics comprise the photomultiplier, amplifier, TDC and ADC and discriminator. A couple of coaxial relays permits switching to electronic calibration. There, a pulse generator - simulating the photomultiplier pulse - and a delay-line (0-64 ns) plus a variable attenuator permit isolation of discriminator and TDC parameters. Another pulse generator is controlled by the station frequency standard and supplies one start pulse and a 1 MHz pulse train for the stop-channel, if triggered by the computer. By range-gating, a TDC test can be performed for longer delays. Although systematics and jitter from the time standard are no longer measured (the same standard is fed to test generator and TDC), an upper limit of the timing jitter of the two TDC verniers (nonlinearity which maps into jitter) still can be judged with this method.
With this setup, the main receiver parameters could be investigated; in fact, with the picosecond laser as optical excitation source a nearly optimal test facility is available in situ. The only facility lacking for pulse analysis and detection strategy optimization is a fast pulse digitizer; here we have to be content with a TEKTRONIX 7834 model oscilloscope plus 7A19 vertical amps's with a combined

---

*) The chopper has not been used up to this date in order to have minimum receiver complexity.

band width/rise time of 400 MHz/.9 ns.
In addition, an external target in a distance of 1.4 km is now and then used for testing beam divergence, telescope pointing and for veryfying the calibration constant.

3. INVESTIGATIONS

Delay Calibration of Light Fibre

The fibre has a length of 211. cm. A first estimate with a speed of light of 18 cm/ns yields a delay of 11.7 ns. Comparing the geometries of the calibration paths (light fibre/direct) we arrive at the empirical formula

$$\Delta t_{LF} = \Delta t_{CAL_{LF}} - \Delta t_{CAL_{DIR}} + 9.16 \text{ ns} \quad (1)$$

On two different occasions, this formula yielded the value

$$\Delta t_{LF} = 11.92 \pm 0.01 \text{ ns} \quad (1a)$$

Reduction of Time of Flight to Geodetical Zero

For ranging, the empirical formula derived from geometry for the correction time-of flight is:

$$2R/c = \Delta t_{SAT} - [\Delta t_{CAL_{LF}} - \Delta t_{LF} + 1.80 \text{ ns}] \quad (2)$$

and with (1a)

$$2R/c = \Delta t_{SAT} - [\Delta t_{CAL_{LF}} - 10.12 \text{ ns}] \quad (3)$$

Calibration Constant vs. Time

The constants which have been applied to the quick look data for the period of May, 15 through August, 31, are tabulated in table C. Three groups of data can be distinguished: 75.1 ± .3 / 75.6 ± .4 / 76.3 ± .3, which are due to the selection of various delays in the constant fraction discriminator. These values are subject to final adjustments.
The procedure of establishing this constant for each pass was the following: In-pass calibration was performed after every 6th range. In post-processing, these values were visually screened. Calibrations from low elevations have been removed because of parasitic pulses from the dome. Then the mean was calculated and inserted for each range (Fig. 5). The reason for this procedure - which does not allow for temporal variations during the pass - was the

lack of pulse charge recordings for this period because of the missing light chopper. This fact means that in-pass calibration was prone to slight systematic errors if the operator did not carefully watch and adjust the variable attenuator. This, because the constant fraction discriminator's dynamic range - with the given amplifier - was not better than 1:10. Improvement are under way, but for the period reported, there would be the only alternative to correct visibly biased values with off-line calibrations of the same date.

Residual Time Walk of the Discriminator

A heavy time-slewing was found for pulse amplitudes below 100 mV (threshold at 30 mV). Appropriate amplifier gain and a threshold of 100 mV were then selected (Fig. 2). Residual time walk was still detectable (Fig. 3, 4) but was found to be sufficiently small for LAGEOS tracking, where seldom returns occured with more than $n = 8$ photoelectrons (Fig. 6). Problems arise with STARLETTE with $n > 60$; and with in-pass calibration runs if the beam attenuation is not closely controlled.

The modelling of the residual time walk is not easily done because of the lack of understanding it's cause. For this reason, leading edge discrimination still appears attractive because of it's bell-shaped response.

4. CONCLUSIONS

In-pass calibration has already proven to be a valuable asset to Zimmerwald LRS. Once the deficiencies of the present setup will be overcome, all calibration points will be corrected for the residual time walk. Then a comprehensive record of the stations internal range bias will be accumulated without the effort of cumbersome pre- and post-pass calibrations to an external target board.

REFERENCES

Silverberg, E.C., 1982 "The Feedback Calibration of the TLRS Ranging System" in Proc. of the 4th International Workshop held at the University of Texas in Austin, Texas, USA

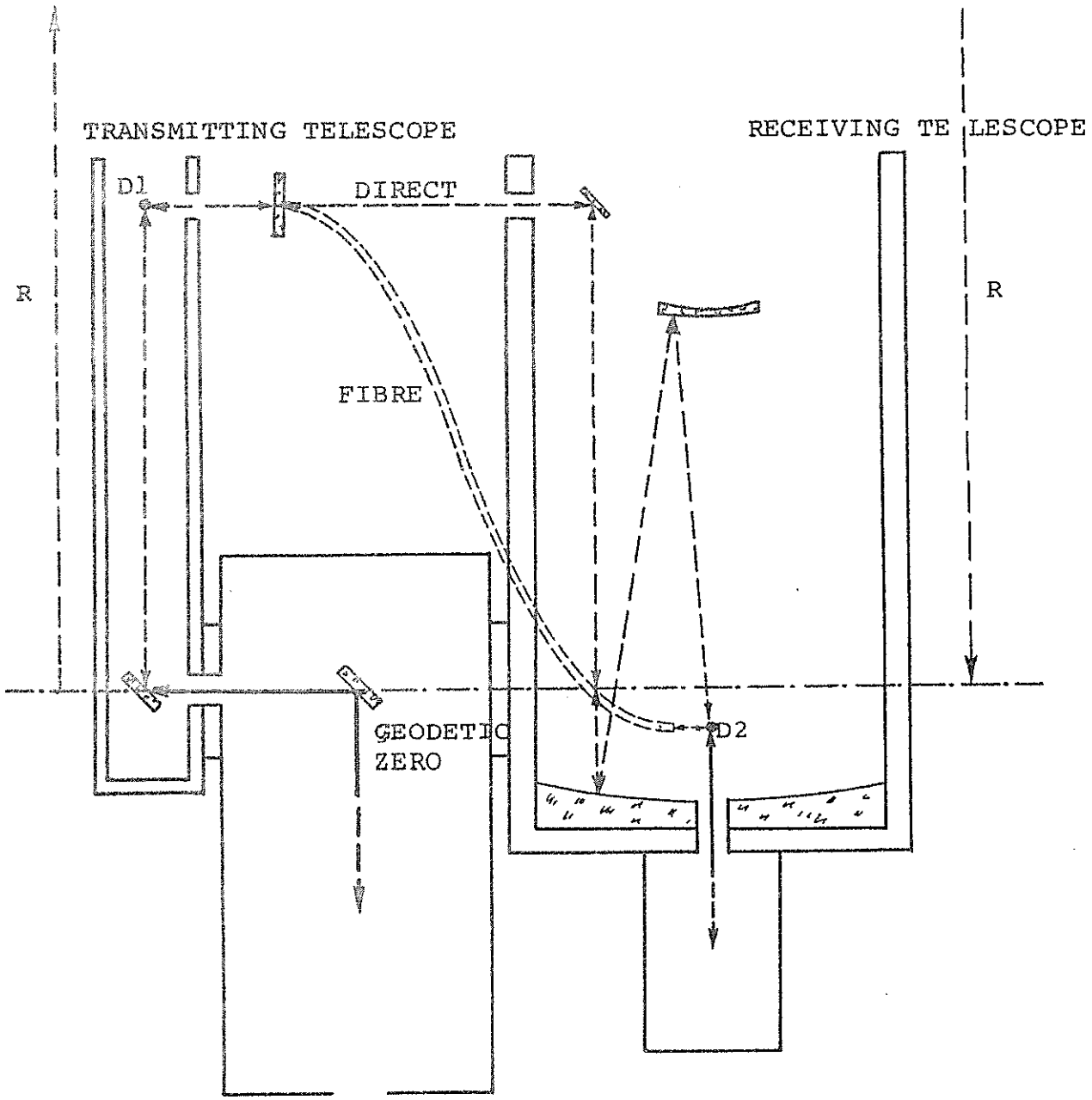

FIGURE 1 THE TWO CALIBRATION PATHS (DIRECT AND LIGHT FIBRE) OF THE ZIMMERWALD L R S.

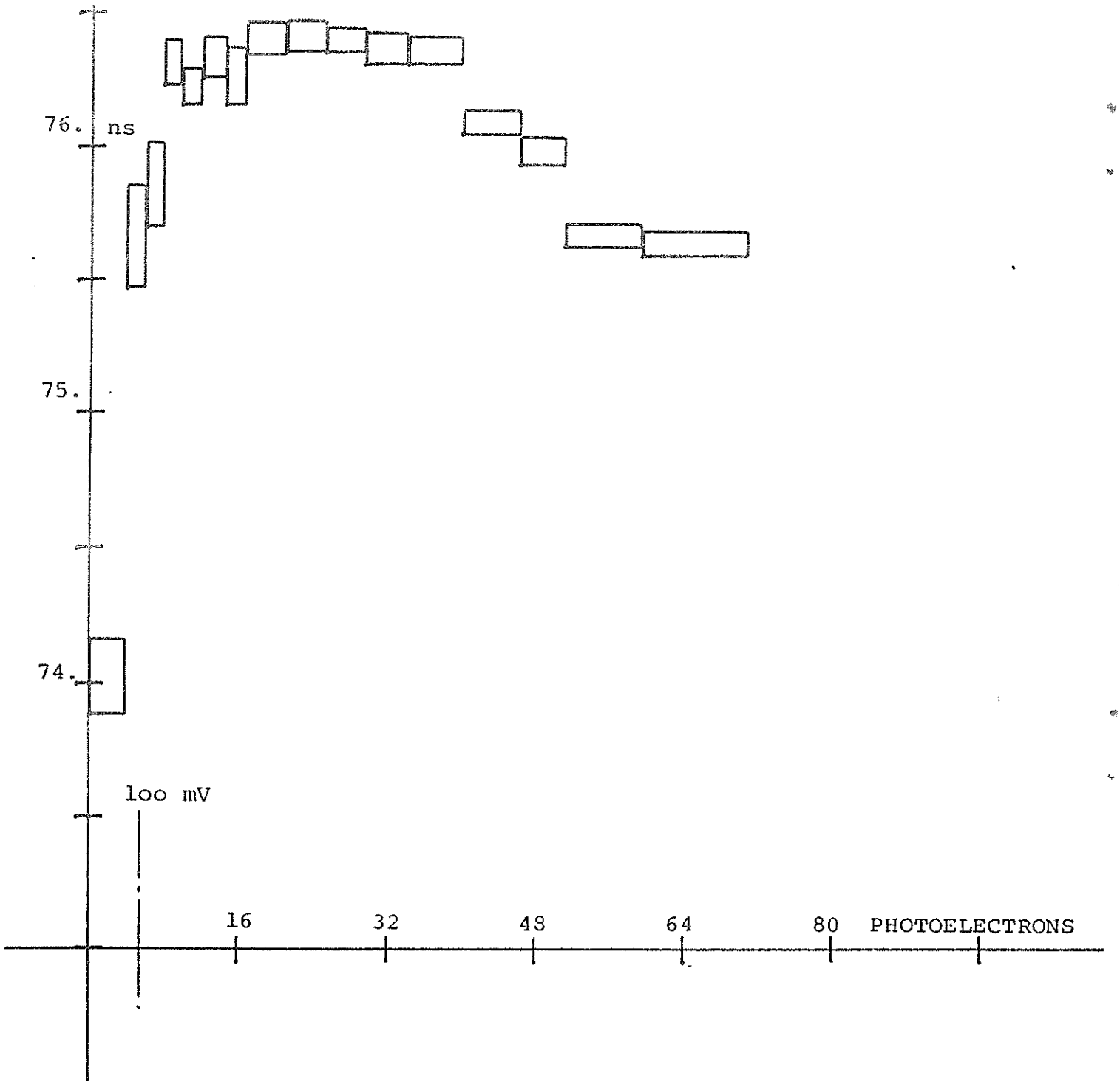

FIGURE 2 TIME SLEWING BELOW 100 mV SHOWS in IN THIS CALIBRATION DELAY VS. PULSE STRENGTH PLOT. ALSO VISIBLE IS TIME WALK STARTING AT 600 mV DUE TO AMP-LIFIER SATURATION

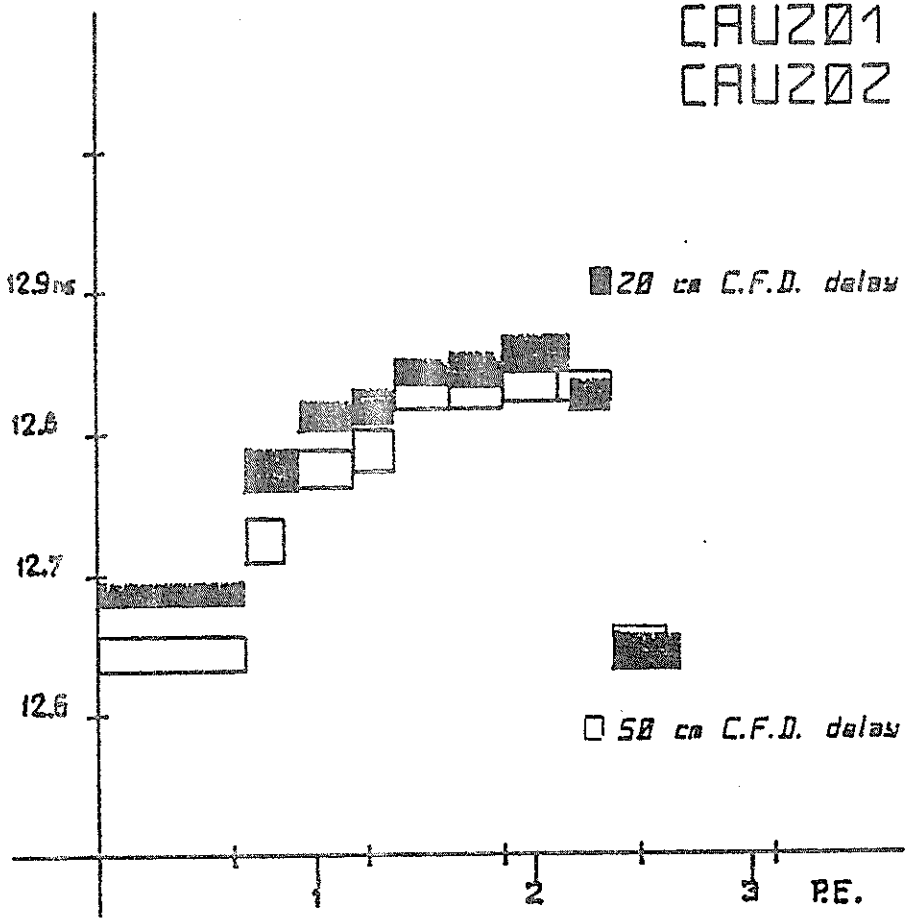

Fig.3 Residual time-walk of constant fraction discriminator vs. photoelectron equivalents. (Few photoelectron regime)

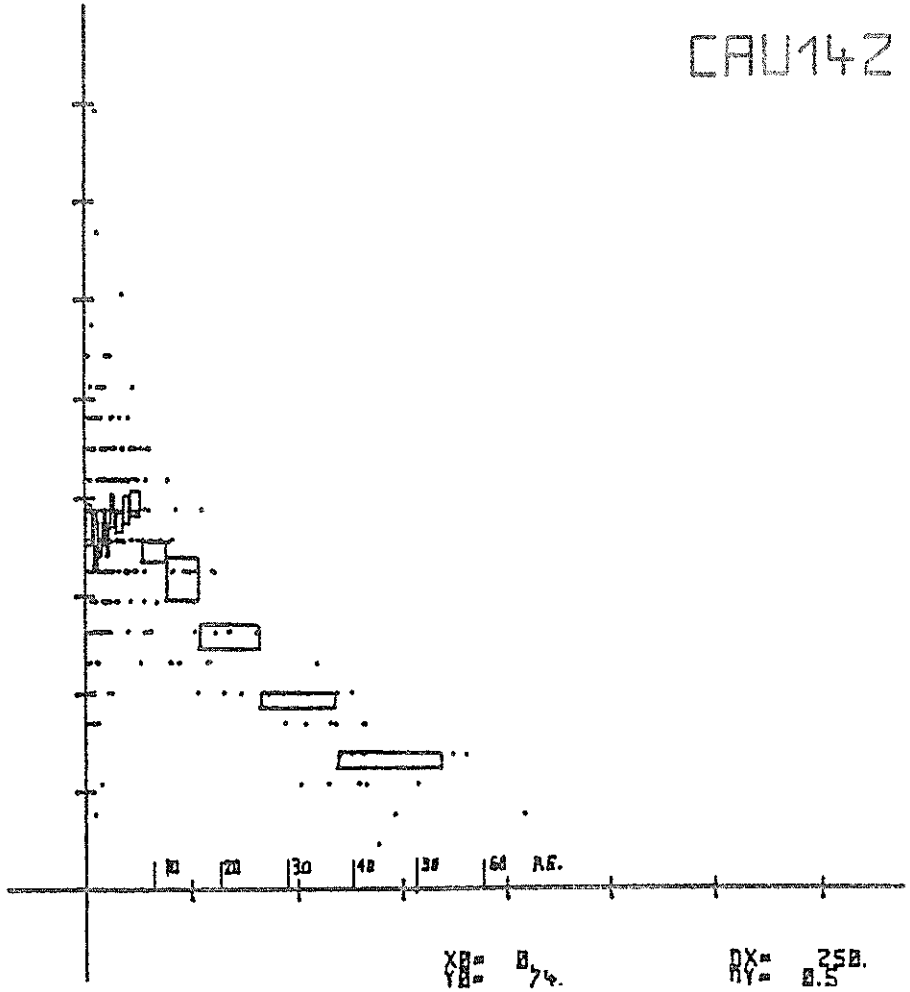

Fig.4 Residual time-walk, multiphotoelectron regime. Note degradation above 15 photoelectron equivalents!

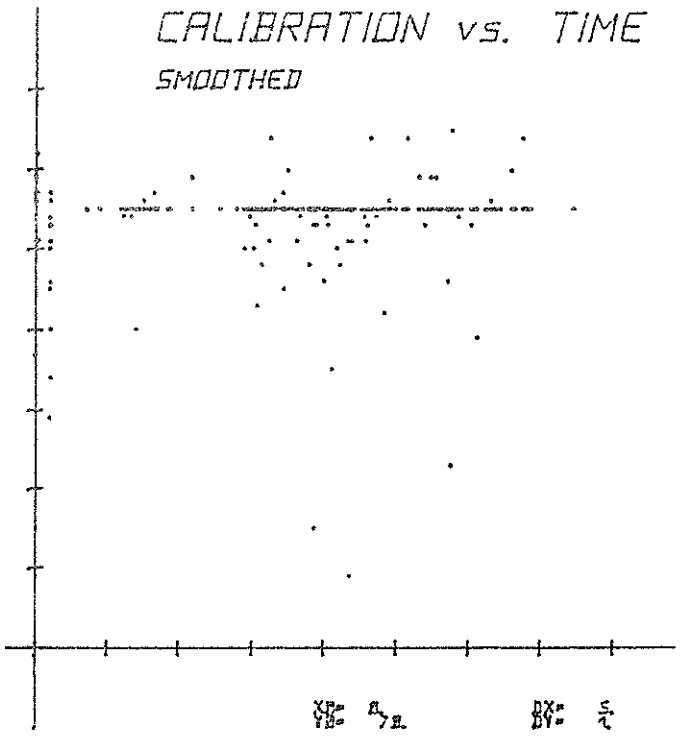

Fig.5 Result of in-pass calibration before and after screening

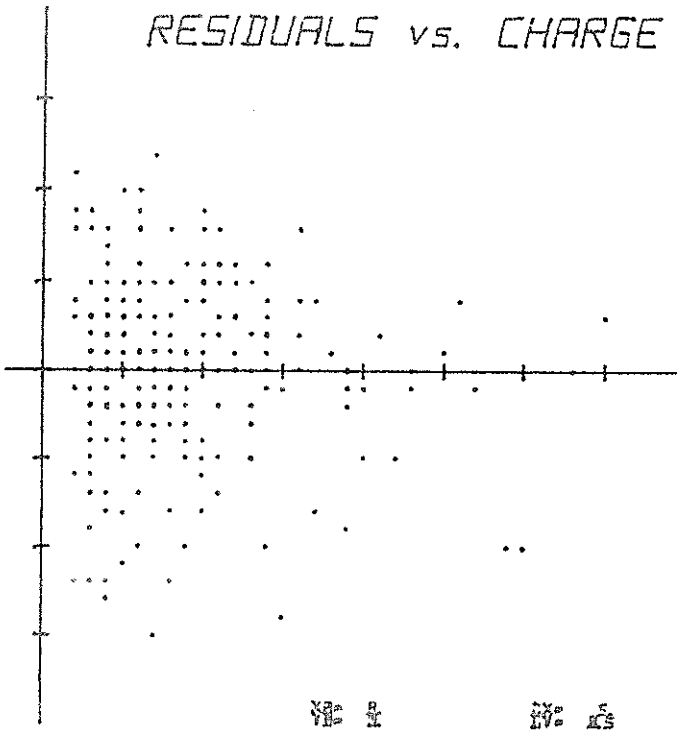

Fig.6 Residuals of LAGEOS-pass after off-line screening vs. return pulse strength.
vert.scale: 7.5 cm/division
hor. scale: 1.2 P.E./div.

LAGEOS	1984- 5-15	1:22	75.6
LAGEOS	1984- 6-16	22:44	74.9
LAGEOS	1984- 6-17	21:27	75.2
STARLETT	1984- 6-17	0:16	75.4
STARLETT	1984- 6-17	20:57	75.0
STARLETT	1984- 6-18	0:37	75.2
LAGEOS	1984- 6-18	0:50	75.2
STARLETT	1984- 6-17	22:47	75.0
STARLETT	1984- 6-18	21:16	75.7
STARLETT	1984- 6-19	0:56	75.4
STARLETT	1984- 6-19	21:36	74.8
LAGEOS	1984- 6-19	22:12	75.0
STARLETT	1984- 6-19	23:26	75.0
LAGEOS	1984- 6-20	1:37	75.0
STARLETT	1984- 6-20	23:46	74.8
LAGEOS	1984- 6-25	21: 8	75.0
STARLETT	1984- 6-25	21:44	75.0
STARLETT	1984- 6-26	22: 4	75.0
LAGEOS	1984- 6-26	23: 9	75.0
LAGEOS	1984- 6-27	21:52	75.0
STARLETT	1984- 6-27	22:25	75.0
LAGEOS	1984- 6-29	22:37	75.2
LAGEOS	1984- 7-17	0: 6	75.1
LAGEOS	1984- 7-17	22:43	75.0
LAGEOS	1984- 7-18	2:16	75.0
LAGEOS	1984- 7-19	23:28	74.9
LAGEOS	1984- 7-20	22: 9	74.8
BEACON-C	1984- 7-21	1:18	75.0
LAGEOS	1984- 7-21	1:39	74.9
LAGEOS	1984- 7-22	22:54	74.8
BEACON-C	1984- 7-22	23:55	74.5
LAGEOS	1984- 7-23	2:33	74.6
LAGEOS	1984- 7-27	23: 7	76.5
LAGEOS	1984- 7-29	20:32	76.1
BEACON-C	1984- 7-29	22:49	76.6
LAGEOS	1984- 7-29	23:59	76.3
LAGEOS	1984- 7-30	22:34	76.3
BEACON-C	1984- 7-30	22: 8	76.6
LAGEOS	1984- 7-31	2:13	76.3
LAGEOS	1984- 8- 2	22: 1	74.9
LAGEOS	1984- 8- 3	1:36	74.9
LAGEOS	1984- 8- 5	21:29	74.9
BEACON-C	1984- 8- 3	21:17	0.1
LAGEOS	1984- 8-14	23:16	75.5
STARLETT	1984- 8-15	1:53	75.9
LAGEOS	1984- 8-15	21:55	75.8
STARLETT	1984- 8-16	0:26	75.8
LAGEOS	1984- 8-16	1:33	75.8
STARLETT	1984- 8-16	2:13	75.6
LAGEOS	1984- 8-16	20:36	75.3
LAGEOS	1984- 8-17	0: 5	75.7
STARLETT	1984- 8-17	0:46	75.4
STARLETT	1984- 8-17	2:33	75.6
LAGEOS	1984- 8-17	22:41	75.9
STARLETT	1984- 8-18	1: 3	76.0
LAGEOS	1984- 8-19	23:36	75.6
STARLETT	1984- 8-20	3:31	75.8
LAGEOS	1984- 8-20	22: 8	75.6
LAGEOS	1984- 8-21	1:52	75.8
STARLETT	1984- 8-21	0:13	75.2
STARLETT	1984- 8-20	1:42	75.7
LAGEOS	1984- 8-21	20:49	75.4
LAGEOS	1984- 8-22	0:21	75.6
STARLETT	1984- 8-22	2:21	75.5
STARLETT	1984- 8-27	21: 2	75.5
LAGEOS	1984- 8-27	23:10	75.5
STARLETT	1984- 8-28	19:33	75.8
STARLETT	1984- 8-28	21:21	76.0
LAGEOS	1984- 8-28	21:48	75.8
STARLETT	1984- 8-29	19:52	75.8
LAGEOS	1984- 8-29	20:29	75.8
STARLETT	1984- 8-29	21:42	76.1
LAGEOS	1984- 8-30	0: 5	76.0
LAGEOS	1984- 8-30	22:35	75.9
STARLETT	1984- 8-31	20:30	75.9
LAGEOS	1984- 8-31	21:14	75.9
STARLETT	1984- 8-31	22:20	76.0
STARLETT	1984- 9- 1	0:14	75.8
LAGEOS	1984- 9- 1	0:53	75.9
LAGEOS	1984- 9- 1	19:58	75.7
LAGEOS	1984- 9- 1	23:24	75.6
STARLETT	1984- 9- 2	19:22	75.8
STARLETT	1984- 9- 2	21:10	75.9
STARLETT	1984- 9- 2	22:59	75.7
LAGEOS	1984- 9- 2	22: 3	75.8
LAGEOS	1984- 9- 3	20:43	75.6
STARLETT	1984- 9- 3	21:30	75.6

Table C In-pass calibration values obtained and submitted with the passes' quick-look selection. These values are subject to final adjustments.

REAL TIME FILTERING OF LASER RANGING OBSERVATIONS AT THE ZIMMERWALD SATELLITE OBSERVATORY

G. Beutler, W. Gurtner, M. Rothacher
Astronomical Institute
University of Berne
Sidlerstrasse 5 CH - 3012 Berne Switzerland

Telephone 31 65 85 91
Telex 32320

ABSTRACT

Since May 1984 a third generation Nd:YAG Laser system is fully operational at the Zimmerwald Satellite Observatory. In order to maximize the number of successful observations a real time data handling based on the Kalman-Filter technique was developed and implemented into the PDP 11/40 computer system of the observatory. Although many simplifications had to be accepted due to the limitations of our small computer system, the algorithm is capable of predicting the signal-travelling times for the next 20 to 40 seconds counted from the last successful observation with a precision typically better than 10 Nanoseconds (ns). These predictions are used to define in real time the range gate (time interval during which the signal detection is active). At present time the width of the range gate may be reduced from originally 2000 to 4000 ns to 200 to 400 ns after the first few returns of a pass, even if the quality of the predicted orbit is rather poor. So far the filter was used only for night time observations. It proved to (a) increase the number of successful measurements and to (b) produce in real time a relatively clean set of measurements for post-processing. These advantages will be even more pronounced for day time observations.

1. Introductory Remarks

The data filter now in use in our observatory is essentially the real time filter presented in {Beutler, 1983}. Since May 1984 this algorithm has been tested with real observations. As only minor changes of the 1983 filter version proved to be necessary, we restrict ourselves to a brief summary of the theoretical background and we put the emphasis on the performance of the filter in practice. The reader interested in mathematical details is referred to {Beutler, 1983}.

2. Statement of the Problem

During the pass of a satellite over the observatory we are measuring the travel times of Laser pulses from the observatory to the satellite back to the observatory. Certainly we detect more returning light pulses if we have a good a priori estimation of the light travel times at the epoch of the observation, because we are then in a position to reduce the range gate to a few hundred nanoseconds, which in turn reduces the number of spurious pulses. These light travelling times are functions of the geocentric position of the observatory and of the orbit of the satellite. If we had perfect station coordinates and perfect orbit predictions, the problem of setting the range gate would be very simple. Before the pass we would produce a table of theoretical light travelling times, and during the pass the range gate could be set according to this table. Unfortunately matters are not as simple as that. Certainly the position of our observatory is known with sufficient precision for this purpose. The same however is not true for the predicted satellite orbits. Therefore - if we want to have good estimates for the light travelling times in real time - we have to update the orbit during the pass of the satellite in real time. This, of course, is a typical Kalman Filter problem. It is even a somewhat simpler problem, because the underlying system equations are ordinary and not stochastic differential equations, the well known equations of motion of the satellite. But even then the

solution of this problem is out of scope for a small computer system. It was shown however in {Beutler, 1983} that the problem can be reduced to a manageable size (a) by using the perturbation equations instead of the original equations of motion and (b) by estimating only one osculating element, the perigee passing time T_0 in real time. With these simplifications the well known matrices of the Kalman Filter theory reduce to scalars. Moreover the celestial mechanics part of the problem, computation of the predicted orbit and its derivatives with respect to the element T_0, are computed off line before the satellite pass.

3. Outline of the Algorithm

The Zimmerwald Filter may be divided into two parts

(a) Initialization phase with $n_I \leq 14$ observations

(b) one filter-step for each subsequent observation

Initialization is a delicate problem in many applications. Here we have the additional problem of a relatively high percentage of parasitical pulses. The normal filter setup (assumption of a large a priori variance for the unknown element T_0) would therefore erroneously interpret many parasitical pulses as real, which would lead to a filter divergence from the very beginning.
Therefore we proceed as follows:

(1) We establish a series of $n_I \leq 14$ measurements with maximum repetition rate (5 Hz).

(2) We compute n_I independent estimates for the improvement of T_0

$$\Delta T_{0,k} = (\Delta t'_k - h(t_k))/\, C(t_k), k=1,2,..,n_I \quad (1a)$$

Where $\Delta t'_k$ is the observed signal travel time,
$h(t_k)$ is the predicted travel time
$C(t_k)$ is the partial derivative of $h(t_k)$ with respect to T_0

$(1)_1$

(3) We form the differences

$$d_{ik} = |\Delta T_{0,i} - \Delta T_{o,k}| \quad , \quad i,k=1,2,\ldots,n_I$$

(4) If $d_{ik} \leq \sigma_i / |C(t_i)|$ for at least n^* different d_{ik}, the initialization process is said to be successful. Otherwise the the whole process has to be repeated from point (1).

(1)$_2$

σ_i and n^* are program parameters. At present time we use the values

$$\sigma_i = \begin{matrix} 50 \text{ ns for Lageos} \\ 150 \text{ ns for Starlette} \end{matrix}$$

$$n^* = 2$$

(2)

The formulae to compute $h(t)$ and $C(t)$ in eqn. (1a) are rather complicated. Therefore a table of these quantities is computed off line before the satellite pass. During the pass $h(t_k)$, $C(t_k)$ are established by interpolation in this table. As the degree of the interpolating polynomial is only 3, the computation of $h(t_k)$ and $C(t_k)$ is <u>not</u> time consumptive.

If the initialization was successful, the subsequent filter steps have to be initialized as follows:

i_0 is the index of the first successful observation

$$\Delta T := \Delta T_{i_0}$$

$$Q := 1/C(t_{i_0})^2$$

$$E := 0$$

$$j := 1$$

(3)

The complete algorithm may then be represented by scheme (4).

THE ZIMMERWALD REAL TIME DATA HANDLING - VERSION 1984

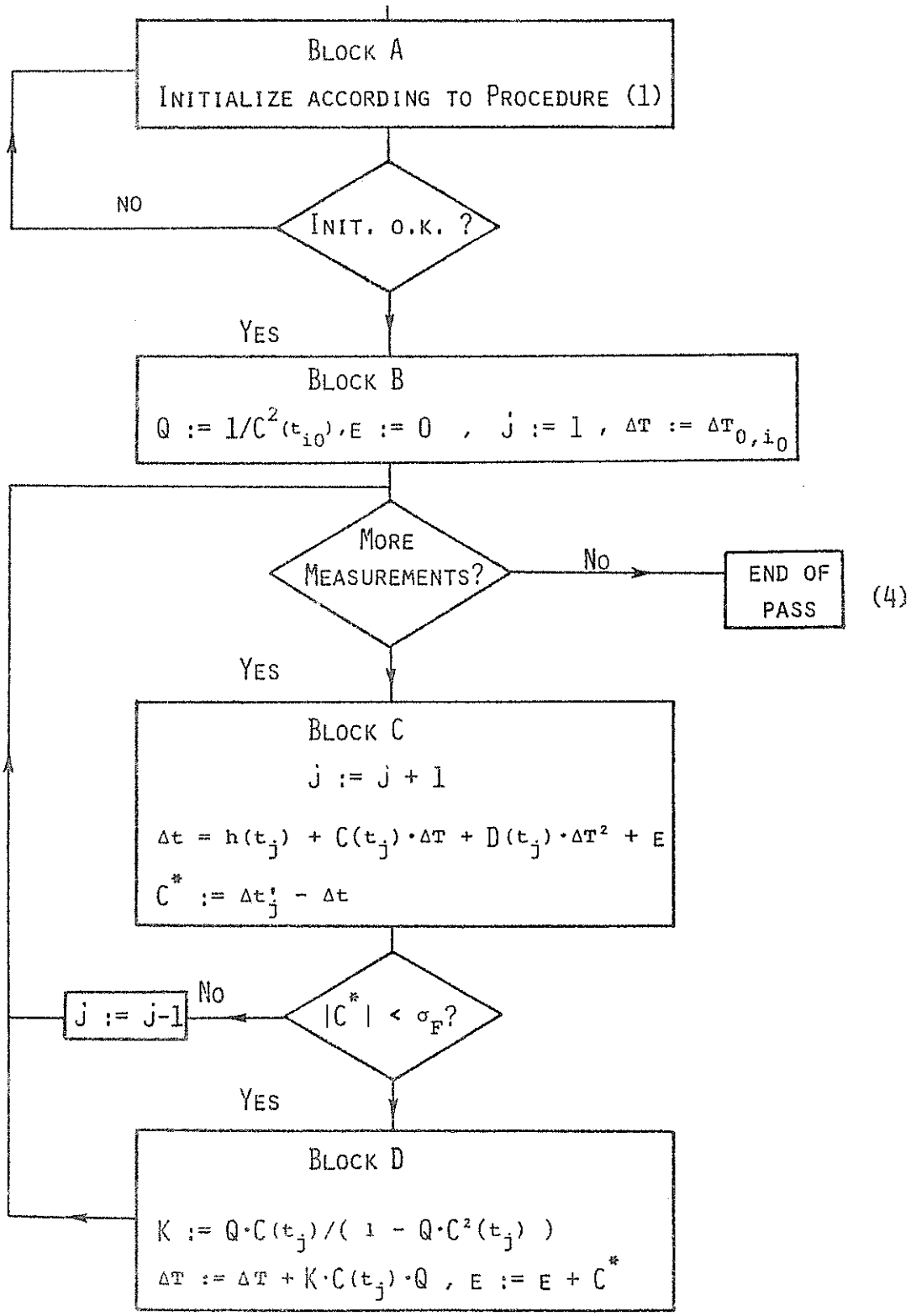

Some remarks concerning scheme (4)

- The prediction of the light travel times Δt in the above scheme differs in two points from the pure Kalman-formulation :
  (a) the quadratic term " $D(t_j) \cdot \Delta T^2$ " is taken into account, where the coefficient $D(t_j)$ is computed in the same way as the quantities $h(t_j)$, $C(t_j)$ in eqn. (1a).
  (b) A very simple empirical correction term E was introduced to prevent the filter from the well known effect of diverging. A full dicussion of this term may be found in {Beutler, 1983, section 5.4.2}.
- σ_F is an input parameter of the program. At present time we use

$$\sigma_F = \begin{cases} 15 \text{ ns} & \text{for Lageos} \\ 50 \text{ ns} & \text{for Starlette} \end{cases}$$

4. Results

Figures 4.1, 4.2 and 4.3 are included to illustrate the filter performance. The three figures refer to the same pass of the satellite Lageos (1984, September 1, 19^h56^m - 20^h29^m U.T.).

Figure 4.1 shows the predicted*) minus the observed light travel times for <u>all</u> measurements recorded (good and faulty). The effect of narrowing the range gate after the initial phase is clearly visible. Clearly the probability to detect the real echo is increased by a factor 5 (initially the range gate width was 2000 ns, after the initialization it could be reduced to 400 ns).

Figure 4.2 shows the residuals of all measurements accepted by the real time filter. The plot was produced by the off line data screening program (no such plots are produced in real time). The residuals therefore refer to an a posteriori optimized orbit. A similar Figure would result however, if we would display the differences "light travel times predicted by Kalman-

*) predicted without a filter, using only the predicted ephemeris

Filter minus observed travel times" for the observations accepted by the Filter algorithm (4). Figure 4.2 also shows that our real time filter produces a relatively clean data set in real time. That there still are some blunders left follows by comparing Figures 4.2 and 4.3 (Figure 4.3 shows the residuals of the measurements finally accepted by the automatic screening program).

So far the real time filter was used for 80 passes (44 of Lageos, 31 of Starlette and 5 of Beacon - C). Usually - as e.g. in the example given by Figures 4 - the real time filter accepts more measurements than the off-line data screening. The opposite may happen, if the operator looses the satellite during the pass and a re-initialization is invoked. Therefore we measure the filter performance by the percentage of wrong real-time decisions "hit yes or no".

Table 4.1

Satellite	Number of Passes	Percentage of wrong decisions
Lageos	44	5.7 %
Starlette	31	8.7 %
Beacon-c	5	3.9 %

5. Conclusions

A very efficient real time data data handling system was developed and tested in the Zimmerwald Satellite observatory. The main difficulty was the reduction of the problem to a manageable size. The first practical experiences are very encouraging.

Reference

Beutler, G. , 1983 "Digitale Filter und Schätzprozesse" , Mitteilung Nr. 11 der Satellitenbeobachtungsstation Zimmerwald, Druckerei der Universität Bern.

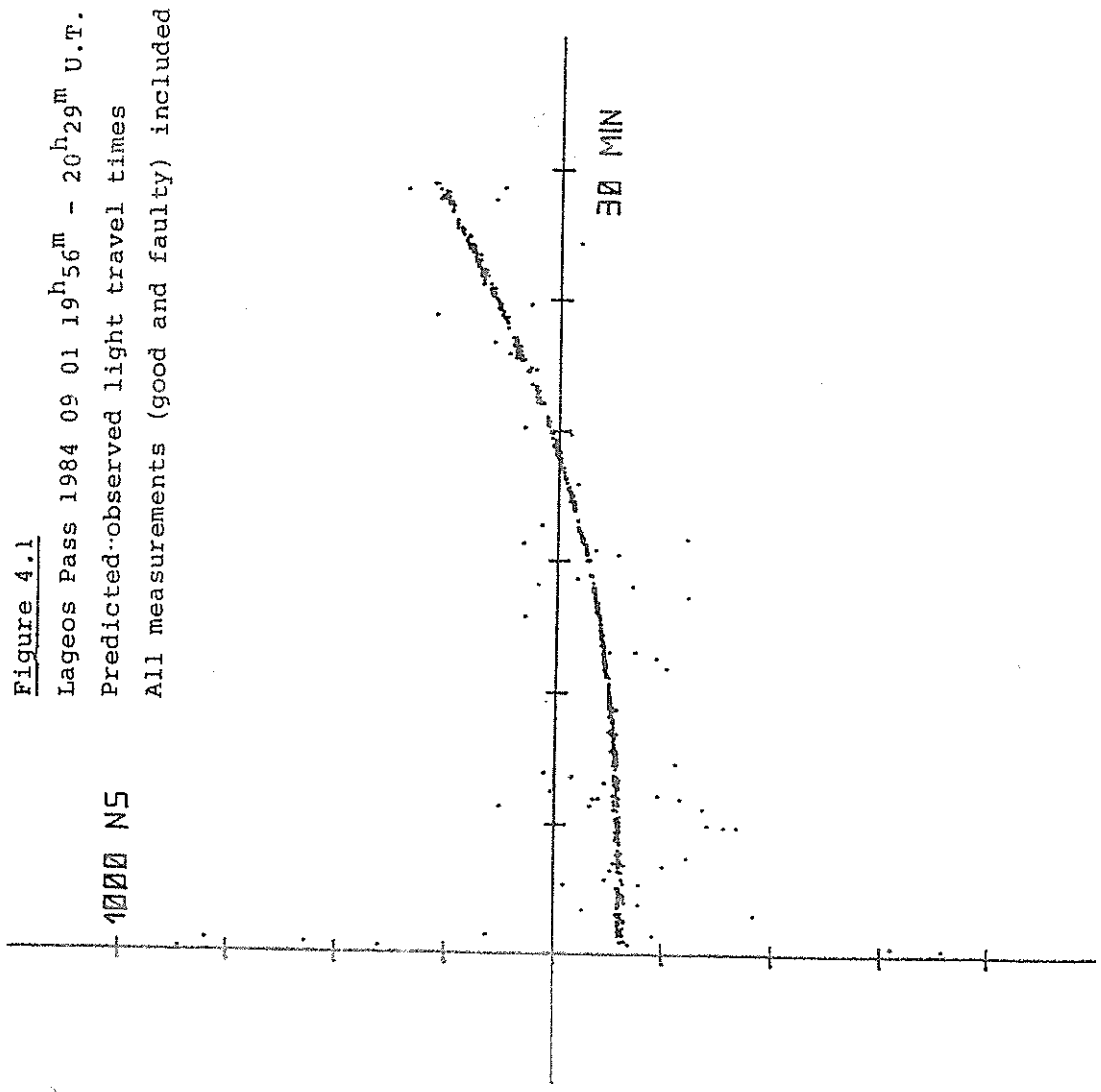

Figure 4.1

Lageos Pass 1984 09 01 19^h56^m - 20^h29^m U.T.

Predicted-observed light travel times

All measurements (good and faulty) included

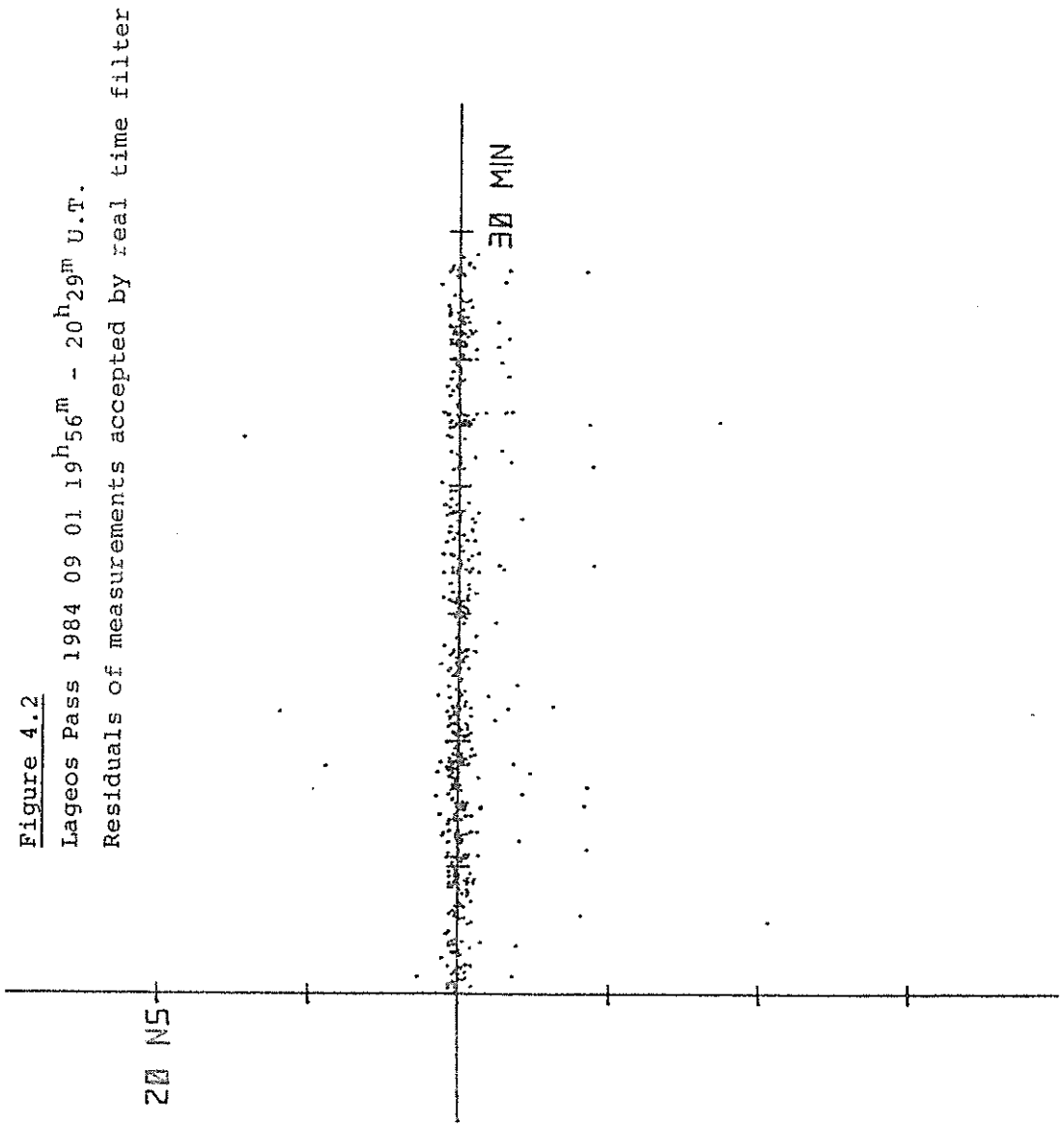

Figure 4.2

Lageos Pass 1984 09 01 19^h56^m - 20^h29^m U.T.

Residuals of measurements accepted by real time filter

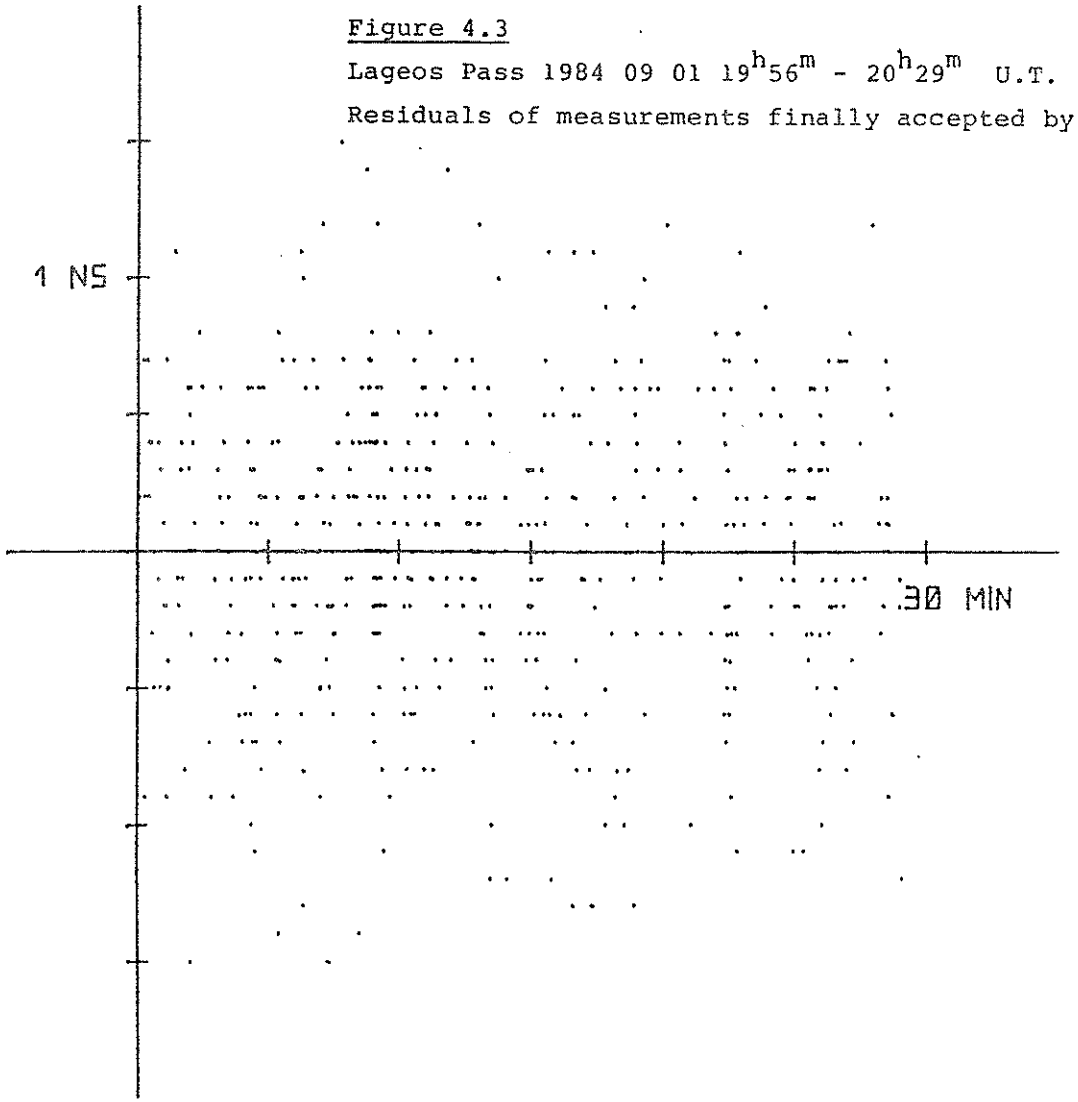

Figure 4.3

Lageos Pass 1984 09 01 19^h56^m - 20^h29^m U.T.

Residuals of measurements finally accepted by off-line screening

Statement of Problem

- Perfect a priori knowledge of light travelling times $\Delta t_i, i=1,2,\ldots$ allow
  - Reduction of range gate width, which
  - increases the number of successful observations

- Only source of incertainty in knowledge of Δt_i is the orbit of the satellite. Therefore we should Improve the orbit in real time using the Kalman-filter-theory.

- Main Contribution of the Zimmerwald Filter is the reduction of this Problem to a <u>manageable size</u> for small computers by
  - Use of perturbation equations instead of Newtonian Equations of Motion
  - Reduction of the number of unknowns from originally 6 to 1 (perigee-passing-time T_0)
- Consequence of these simplifications : All Matrices in Kalman-Theory are reduced to scalars, which speeds up on line computations essentially.
- Initialization : A special procedure related to the majority - voting in Doppler observations was developed: The first 10 - 14 observations are used to produce 10 - 14 independent estimates of T_0. If - within the expected variances of the measurements - 3 or more coincidences are found, the initialization process is said to be successful.

INTERKOSMOS LASER RADAR, VERSION MODE LOCKED TRAIN

K. Hamal, H. Jelinkova, A. Novotny, I. Prochazka
INTERKOSMOS
Faculty of Nuclear Science and Physical Engineering
Czech Technical University
Brehova 7, 115 19 Prague 1 Czechoslovakia

Telephone (2) 84 8840
Telex 121254

ABSTRACT

To obtain the system internal noise level below 10 cm at the INTERKOSMOS laser radar in Helwan, the picosecond laser was implemented. The Nd YAG oscillator/amplifier/SHG laser generates a mode locked train at 0.53 μm, most of the energy is contained in three pulses, the individual pulse duration is 70 psec. During the 1983 Merit Campaing, within 4 months, 100 low satellite passes and 31 Lageos passes have been ranged. When the mode locked substructure has been resolved for the received signal (about 50 % of passes), the RMS was 6-8 cm.

INTERKOSMOS LASER RADAR,VERSION MODE LOCKED TRAIN

The INTERKOSMOS 2.generation laser radar /1/ located at Helwan has been operating since December 1980. Satellite ranging data having RMS 20 cm, obtained during the preliminary MERIT campaign /September 1981/, using 5 ns ruby laser, showed acceptable consistency with other data /3,4/.

To obtain the RMS below 10 cm level we adopted a picosecond mode locked train laser /2/. Assuming the space available for the transmitter /two axe mount, moving transmitter/, we have chosen the mode locked train Nd:YAG oscillator/amplifier/ SHG laser system /5/. The oscillator is passively mode locked- the individual pulse length is 70 psec, the round trip time is 2nsec, most of the energy is concentrated in two or three pulses of the train.

The station has been upgraded to exploit the mode locked train /6/, the software package for the ranging data processing has been developed /7/.

The system block scheme is on Fig.1., the main parameters are summarized on the table 1.

To improve the mount positioning accuracy, the aiming errors model was implemented. The transmitted beam divergence is adjustable by means of a transmitting optics /from 0.2 to 3 mrad/. The receiver PMT is cooled to decrease its single PE dark count rate. The Start dezector /8/ was adopted to proceed the train of transmitted pulses. Two wideband preamplifiers and the constant fraction discriminator were implemented into the Stop channel to guarantee a low jitter on sigle PE level. The epoch timing counter resolution is 1 us. As the epoch reference, the Loran-C signal is used, the computerised comparison procedure of the station time base to the Loran signal was put into operation. The signal propagation delayes were calibrated by the flying Cs clock. The computer hardware/software control package was modified to accept the ranging reprates up to 5 pps, the on line graphics capability was implemented.

The indoor calibration experiment /9/ showed the ranging electronics interval noise 6 cm /RMS/.

During the 1983 MERIT campaign 100 low satellites and 30 Lageos passes have been ranged within four months. When the mode locked substructure has been resolved in the received signal /50% of passes/, the RMS 6-8 was achieved. The system stability /10/ /pre-post pass calibration difference/ is typicaly 2.5 cm. The average data rate is /1/ Lageos return every /30/ seconds.

TECHNICAL PARAMETERS OF THE INTERKOSMOS LASER RADAR IN HELWAN VERSION MODE LOCKED TRAIN

MOUNT	CONFIGURATION	AZIMUTH/ELEVATION
	TRACKING RATE	ZERO TO ONE DEG/SEC
	POINTING ACCURACY	30 ARCSEC
TRANSMITTER	LASER TYPE	Nd:YAG + SHG
	OPERATIONAL	MODE LOCKED TRAIN
	ENERGY	15 mJ/TRAIN
	PULSE LENGTH	70 PSEC
	ENVELOPE FWHM	4 NSEC /2-3 PULSES/
	REPRATE	2.5 PPS
	OUTPUT BEAM DIVERGENCE	ADJUSTABLE 0.2-2. mrad
RECEIVER	OPTICS	REFRACTOR, 0.4 METER
	BANDPASS FILTER	1 nm
	PHOTOMULTIPLIER	RCA 31034A,GATED,COOLED
RANGING ELECTRONICS	DISCRIMINATOR START	SPECIAL
	DISCRIMINATOR STOP	CONSTANT FRACTION
	FLYING TIME COUNTER	100 PSEC RESOLUTION
	TIME GATE	100 NSEC RESOLUTION
EPOCH TIMING	RESOLUTION	1 MICROSECOND
	FREQUENCY STANDARD	Cs BEAM FREQUENCY STD
	EPOCH REFERENCE	LORAN C,FLYING CLOCK
COMPUTER	CPU	FLOATING POINT
	MEMORY CAPACITY	64 KBYTES
	STORAGE MEDIUM	5 MBYTE DISC
	I/O FACILITIES	PAPER TAPE,PRINT
		GRAPHICS CAPABILITY
		HP CASSETTES, HP-IB
SOFTWARE	PREDICTION	0.2 ARCMIN ACCURACY
		ON SITE IMPROVEMENT
	CALIBRATION/TRACKING	COMPUTER CONTROLLED
	DATA PROCESSING	NOISE REJECTION
		ML TRAIN DATA ANALYSIS

Table 1.

L i t e r a t u r e

1/ K.Hamal,H.Jelinkova,A.Novotny,I.Prochazka,M.Cech,Interkosmos Second Generation Satellite Laser Radar,proceedings of the Fourth International workshop on Laser Ranging Instrumentation Texas,Austin,USA,published in Bonn,1982
2/ E.C.Silverberg, The Feedback Calibration of the TLRS Ranging System, in /1/, Vol II,p 331
3/ S.D.Tapley,B.E.Schutz,R.J.Eanes,A Critical Analysis of Satellite Laser Ranging Data, in /1/,Vol II,p 523
4/ J.H.Latimer J.M.Thorp,D.R.Hanlon,G.E.Gullahorn,A Review of Network Data Handling Procedures, in /1/, Vol I, p107
5/ H.Jelinkova, Mode Locked Train Laser Transmitter in this Proceedings
6/ I.Prochazka, Mode Locked Train Laser Ranging Data Processing, in this Proceedings
7/ A.Novotny,I.Prochazka, Upgrading the Computer Control of the Interkosmos Laser Ranging Station in Helwan, in this Proceedings
8/ M.Cech, Start Discriminator for the Mode Locked Train Laser Radar,in this Proceedings
9/ K.Hamal,I.Prochazka,J.Gaignebet, Mode Locked Train YAG Laser Calibration Experiment, in this Proceedings
10/ M.R.Pearlman,N.Lanham,J.Thorp, J.Wohn,SAO Calibration Techriques, in /1/, Vol.II,p 323

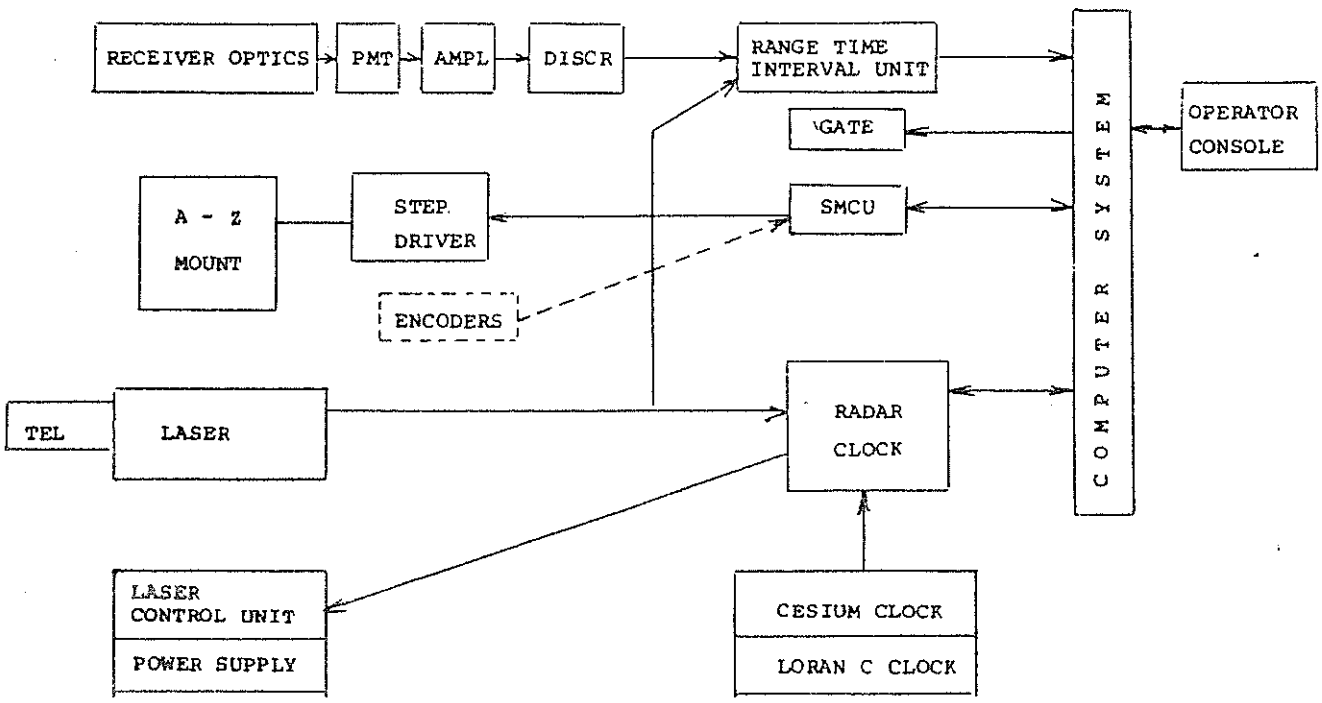

System block scheme

Fig. 1.

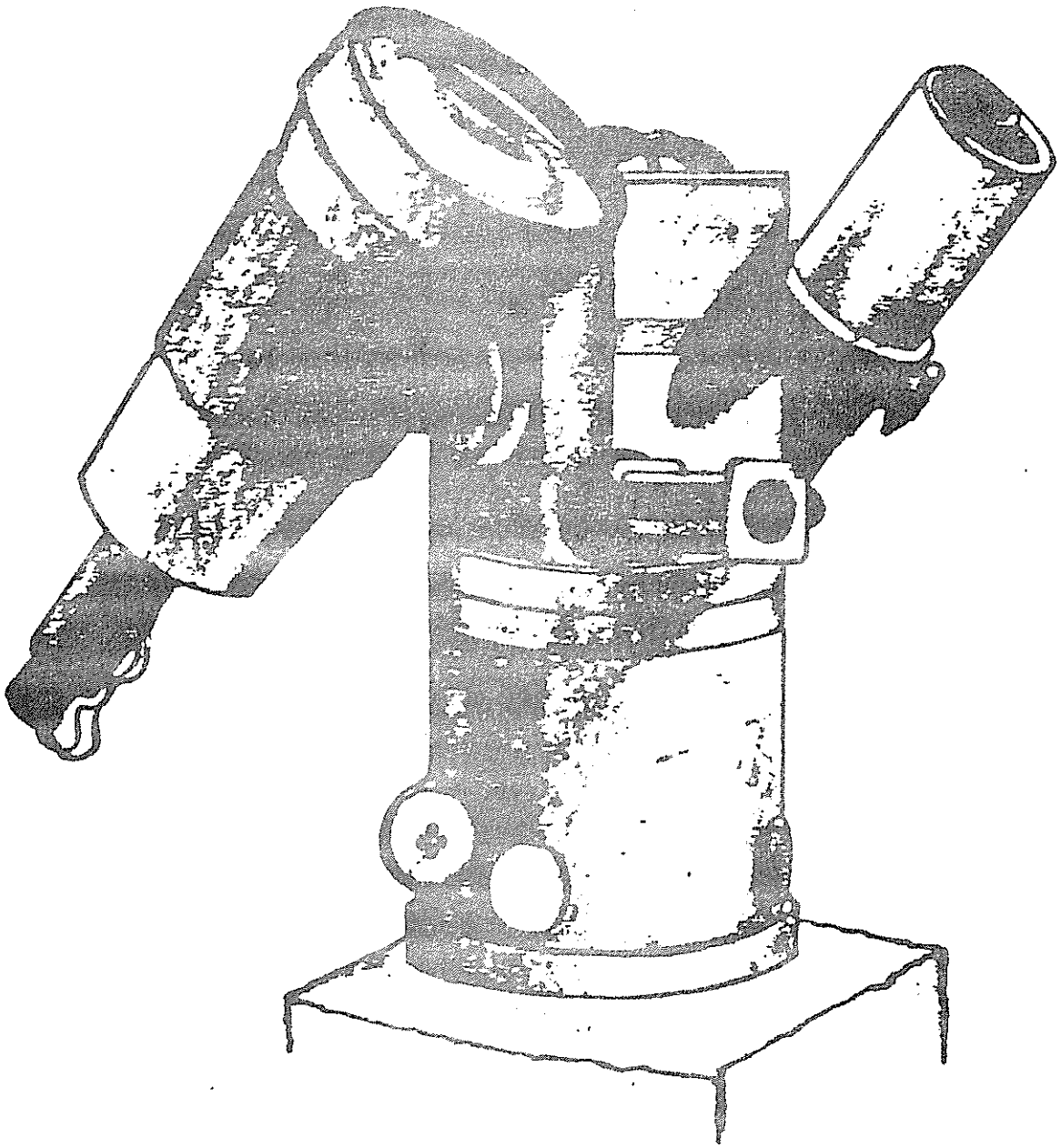

View of the mount/laser/receiver subsystem

START DISCRIMINATOR FOR MODE LOCKED TRAIN LASER RADAR

M. Cech
INTERKOSMOS
Faculty of Nuclear Science and Physical Engineering
Czech Technical University
Brehova 7, 115 19 Prague 1 Czechoslovakia

Telephone (2) 84 8840
Telex 121254

ABSTRACT

A problem of start detector is very topical in laser radar sation working with a train of pulses generating by mode locked Nd:YAG laser. This article deals with new developed start detector used in INTERKOSMOS laser radar station in Helwan, Egypt. A time resolution of the detector is better 150 ps.

START DISCRIMINATOR FOR MODE LOCKED TRAIN LASER RADAR

The start pulse for the time interval counter is generated by detecting a small part of laser beam in a start detector.

The described start detector consists of three part (fig. 1). In the first part, a silicon planar PIN photodiode HP4207 as detection element is used. The photodiode is connected to -150V bias to obtain very fast response.

The second part is a discriminator. The discriminator consists of tunnel diode (TD). The TD is connected as monostable multivibrator. The threshold of discrimination is set up by the level of the multivibrator.

The third part is amplifier, the output voltage from TD discriminator is 100-200 mV. The gain of the amplifier is approximately 20. The first stage is amplifier with common emitor (trans. T1) and second transistor is connected as current amplifier. The rise time is 4 ns and voltage output is 4V. The rise time is suitable for our application (uniform pulse).

The detector works as fixed threshold discriminator. This fact is not important because of rise time 200 ps and change of amplitude is 50% only. The theoretical error of the detector is 100ps only.

We have train of pulses - fig.2. (approx. 2-3 pulses). A problem is in defining the triggering pulse. The detector sends uniform trigger pulse, when the first laser pulse reaches threshold of discriminator. If we take as reference point the maximum pulse in train, it can be triggered from different pulses in respect to this point. The time of triggering is different but this time differes at resonator round trip time. (1.8 ns in our case).

Both stability and accuracy of the start detector were measured. The following measuring configuration was used: a laser pulse was divided into two parts. One part was detected by photodiode and entered to vertical amplifier of the Tektronics 7912AD oscilloscope. Second part of light pulse was processed by start detector. Output pulse from start detector externally triggered the oscilloscope.

Fig.2. shows the overlap of three pulses. Approximately 100 pictures were taken. These pictures were processed by computer. Two different parameters were studied.

The first parameter is the distance of reference point (the center

of maximum peak) from trigger pulse. We can see on the fig.3. that detector generates trigger pulse from the same peak in train in 85% cases, from second one 15% only. Distance between pulses there is 1.8ns.

Second parameter is a time resolution. Fig.4. was obtain by separating one pulse from fig.3. The time resolution of this detector is better then 150ps.

Conclusion

The start detector described in this article is very simple. The reference point obtained by the detector has the time resolution better 150ps. A one resonator round trip time (1.8ns) offset of the reference point is observed in 15% cases. The detector is used by investigation of mode locked lasers as triggering element of oscilloscopes, streak cameras, etc.

Literature:

1/ M.Jelinkova, in this proceedings

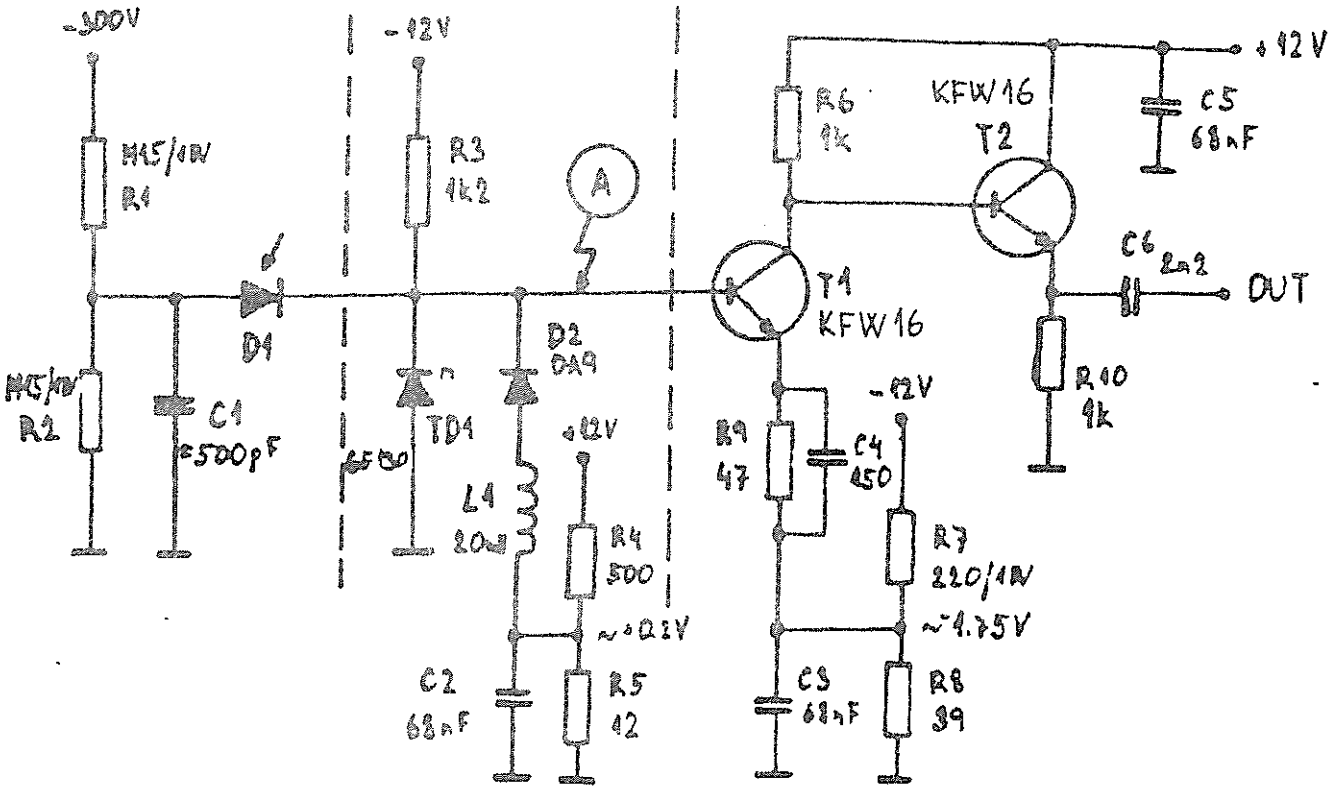

Fig.1.: Circuit diagram of the start detector

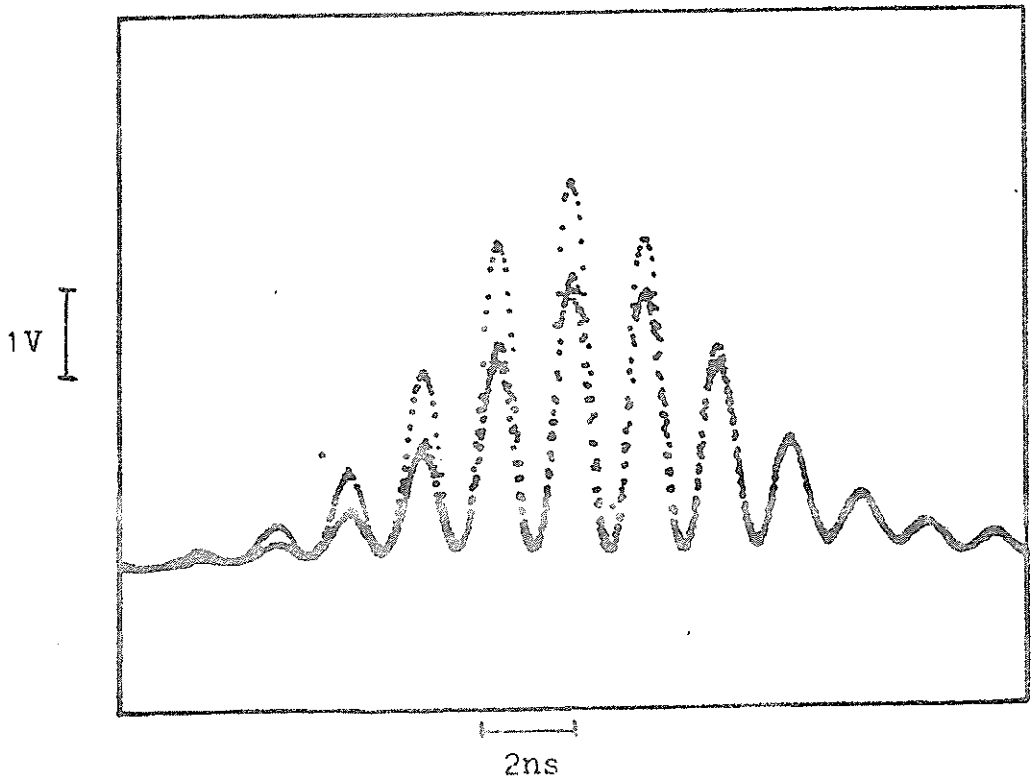

Fig.2.: The overlap of three pulses

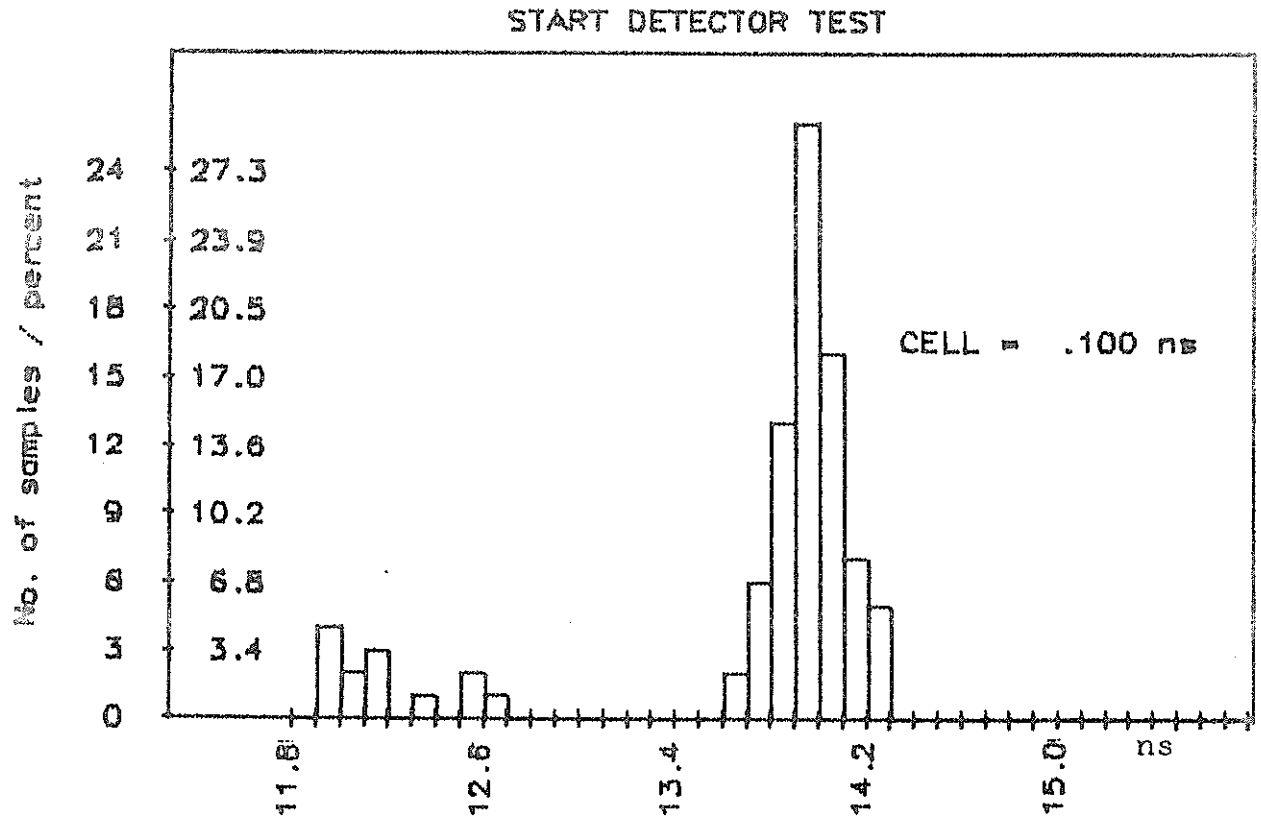

Fig.3.: The position of maximum peak from trigger

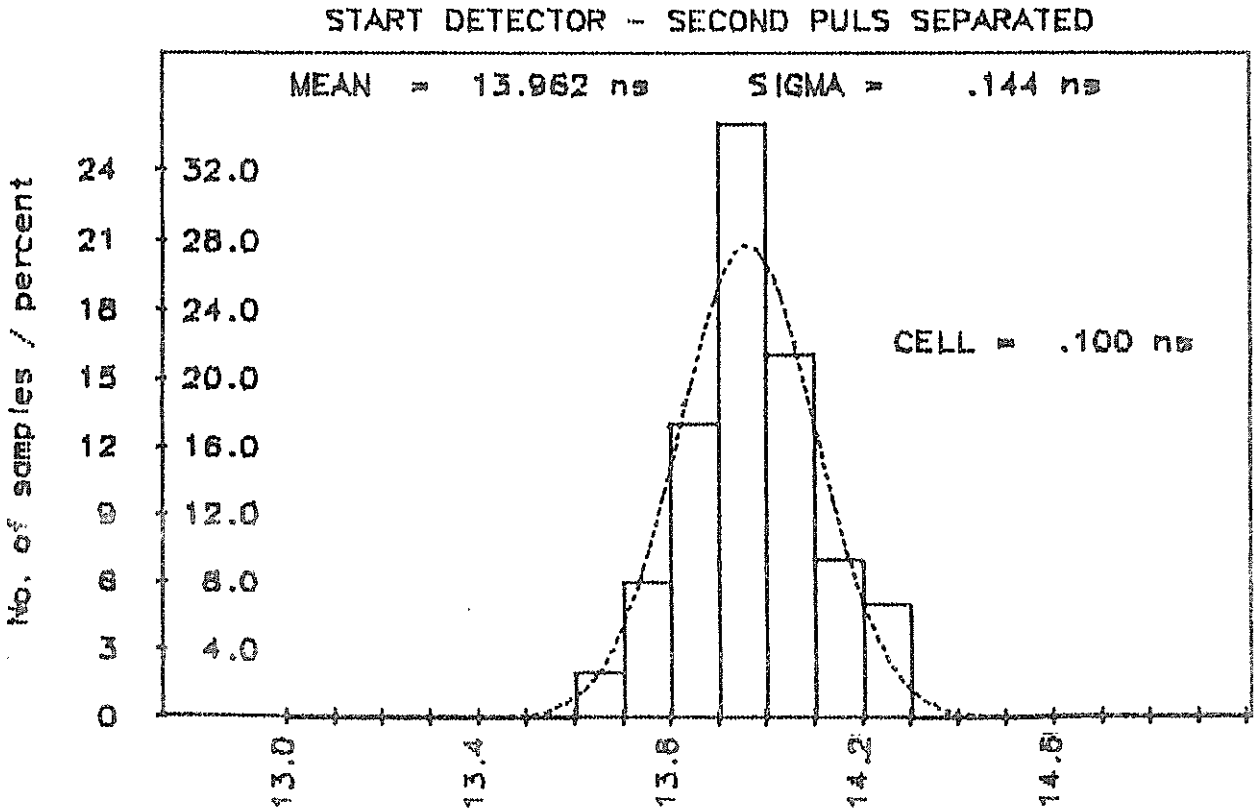

Fig.4.: The time resolution diagram

MODE LOCKED TRAIN LASER TRANSMITTER

J. Jelinkova
INTERKOSMOS
Faculty of Nuclear Science and Physical Engineering
Czech Technical University
Brehova 7, 115 19 Prague 1, Czechoslovakia

Telephone (2) 84 8840
Telex 121254

ABSTRACT

The passively mode locked frequency doubled Nd:YAG oscillator/amplifier/SHG laser radar transmitter is dercribed. It is generating a train of 2-3 pulses, the pulse duration is 77 psec, output energy in green is 20 mJ, the reprate 1-2.5 Hz. The stability of the output pulses was monitored and statistically treated using a computer. To analyse the laser beam structure, an on line diagnostic chain, giving a three dimensional graphic display of the output pattern, was implemented.

MODE LOCKED TRAIN LASER TRANSMITTER

1.0 INTRODUCTION

Considering satellite ranging, the length of the transmitted laser pulse is one of the main parameters, determining the accuracy of the measurements. To increase this accuracy, in the course of years, the pulse width of the transmitted light was shortened. Since 1973, when the Interkosmos laser radars have started to work, a total number of 30 laser transmitters have been put into the laboratory and field operation. Among the transmitters, there was a ruby Q-switched using either rotating mirror or Pockels cell generating the pulses from 13-25 nsec FWHM, PTM Q-switched (cavity dumped) ruby system having 6 nsec pulse width and constant gain pulse forming configuration varying in pulse width from 2-6 nsec /1/. In 1982 mode-locked Nd:YAG laser transmitter generating a train of pulses has been installed at the observatory Helwan in Egypt.

2.0 SYSTEM OF LASER TRANSMITTER

The laser system consists of TEMoo oscillator plus a single pass amplifier, followed by a frequency doubler. The specifications result from the demands of the accuracy in ranging and from the necessity of the system movability /2/. The technical parameters of this system are shown in Tab.1 and a schematic drawing in Fig.1.

Tab.1. TECHNICAL DATA OF THE LASER TRANSMITTER

Wavelength	530 nm	Output divergence	0.2 mrad
Pulse duration	77 psec	(Adjustable)	MIN
No.of pulses	2-3/train	Dimensions length	120 cm
Output energy	20 mJ/train	diameter	23 cm
Reprate	1-2.5 Hz	Power supply /5/	500 W
		(Average power)	

2.1 Laser Oscillator

The deterministic build up of passive mode locking in giant pulse lasers can be achieved by careful control of lasing modes between the first and the second threshold /3/. Stable stationary

pulse train solutions were found for passively mode locked systems with easily saturable active medium. The autors /4/ used the intraresonator telescope to improve the output pulse reproducibility of Nd:YAG system. In our system, the number of modes was reduced by the gain excess and by increasing the intermode frequency spacing via shortening the optical resonator length.

The configuration of the mode locked Nd:YAG oscillator, we employed, is shown in Fig.1. As the active medium, a 80 mm long, 6 mm in diameter, Nd:YAG crystal is used, one end is cut at angle 89° and second one is perpendicular to the axes. The crystal and the flashlamp are placed in the elliptical silver coated cavity. The optical resonator is formed by the high reflectivity (R=99%) dielectric mirror and the perpendicular surface of the Nd:YAG crystal (R=8%). Mode locking is accomplished using a saturable dye ML51 solved in dichlorethane /6/, innitial transmission T = 35%, thickness of the cell is 5 mm. The cell is at the Brewster angle near the 99% mirror. Using a 5 mm saturable dye cell the pulse duration was lengthened. Single mode operation is performed by the aperture (diam.1 mm) placed between YAG crystal and the saturable dye. The length of the resonator corresponds to 2 nsec round trip time. The shape and the reproducibility of the oscillator pulses are remembered in the section 3.

2.2 Amplifier, Doubler and Detection

In the amplifier, a 120 mm long, 6 mm in diameter, Nd:YAG crystal is used, both ends are cut at 2° and antireflection coated. The crystal is placed in the elliptical silver coated cavity and it is pumped by one linear Xe flashlamp. Both crystals, oscillator and amplifier one, and the flashlamps also are placed in a water cooled glass tubes. To isolate the oscillator from the amplifier, the saturable dye cell containing ML 51 disolved in dichlorethane is used. To extend 1 mm oscillator spot, the telescope 1:3 is placed between the oscillator and the amplifier head. For purpose of the laser radar, the generation of the second harmonic is needed. The KDP crystal, type II, is used behind the amplifier. The output pulse is monitored by a high speed photodiode. A sample of the output beam is sent to the start detector /7/. The output telescope changes divergence of the beam. A He-Ne laser is incorporated into the system for easy alignment of the oscillator/amplifier chain and the pointing services. The whole optical system is protected by a removable tight dust cover.

3.0 LASER PERFORMANCE

The experimental setup for measuring of the output pulse reproducibility and the beam structure is in Fig.3.

3.1 Pulse Shape

The typical pulse shape is shown in Fig.2. The train has 2-3 pulses, the pulse separation is 2 nsec and the individual pulse width is 77 psec.

3.2 Pulse Energy and Divergence

The oscillator pulse energy is about 7 mJ/train in infrared. After the amplification, 80 mJ output beam is entering to SHG crystal, the conversion efficiency is 25%, the output energy per train at 0.53 μm is 20 mJ.

The divergence of the system is 2 mrad. The output Galileo adjustable telescope allowes to achieve the output beam divergence up to 0.2 mrad, minimum.

3.3 The Output Pulse Reproducibility and Beam Structure

The shot-to-shot reproducibility and the stability of the output pulses are of the primary importance in satellite ranging. The irregularity of the pulse may impair the timing accuracy. Therefore, the detailed tests of the laser transmitter stability and pulse reproducibility were carried in the indoor experiment. The experimental setup is in Fig.3. The first part is for measuring the stability of the pulse width of the individual pulses and the signal to noise ratio, the second part is for pulse train stability test and third one for beam structure measurement.

The laser pulse was detected by PIN photodiode and Tektronix Tranzient Digitizer 7912AD. The bandwidth of the system was 500 MHz, effective resolution 20 psec. The measured raw data were transmitted via HP 85 to the master HP 21 MX-E computer, processed and stored on the magnetic disc. The laser was operating at 2.5 Hz and 100 from the 100 000 shots consequence were put to the memory and processed. The corresponding software package consists of the programs for data collection and storing, noise elimination, pulse characteristics determination, statistics and graphics /9,10/. The results are in Fig.4.

A part of the laser output pulse is sent to Hammamatsu streak camera system. For data recording and processing, HP 85 calculator was interfaced to the Hammamatsu system (Fig.2). The mean value of the individual pulse width from the 100 measurements is 77 psec, RMS is 10 psec.

The far field structure was studied in the focal plane of the positive lens. As the detector, the Fairchild CCD camera was used. The camera signal was digitized and stored in the Digital Image Memory Quantex with the resolution 256x256 cells 256 intensity levels each. The data from the memory were transmitted via HP-IB to the HP 21 MX-E computer and stored on the disc. The extensive software package /10/ for TV image processing is available in the "nearly on-line" mode. The beam profile etc. was available within seconds after the laser shot

on the monitor in the lab. The Fourier two dimensional transform of the far field structure was available within minutes.

The focal length of the positive lens used for far field image was 2.5 m. In Fig.5, there is the plot of the 3D projection of the far field beam structure of the oscillator (1.06 μm) (a) and the contours (b). The far field beam structure of the transmitter (osc/ampl/doubler) chain is in Fig.6. The output beam divergence is 2 mrad.

4.0 CONCLUSION

The system has been operating in Helwan observatory (Egypt) through the summer 1983 and 1984. The target and satellite ranging shows RMS bellow 10 cm /11/.

REFERENCES

/1/ H.Jelinkova, Proceedings of the Fourth International Workshop, Austin, USA, 1981

/2/ K.Hamal etal., in this Proceedings

/3/ C.P.Auschnitt, IEEE Journal of Quantum Electronics, QE-13,321,1977

/4/ A.N.Zherikhin, V.A.Kovalenko, Kvantovaja Elektronika 2, 377,1974

/5/ V.Kubecek, M.Klasna, FJFI Preprint Series No.83/203

/6/ K.Hamal, V.Hruskova, H.Jelinkova, FJFI Preprint Series No.83/204

/7/ M.Cech, In this Proceedings

/8/ I.Prochazka, FJFI Preprint Series No.83/188

/9/ K.Hamal,I.Prochazka,M.Cech,P.Valach,H.Jelinkova,A.Novotny, FJFI Preprint Series No.83/194

/10/ P.Valach, FJFI Preprint Series No.83/197

/11/ I.Prochazka, In this Proceedings

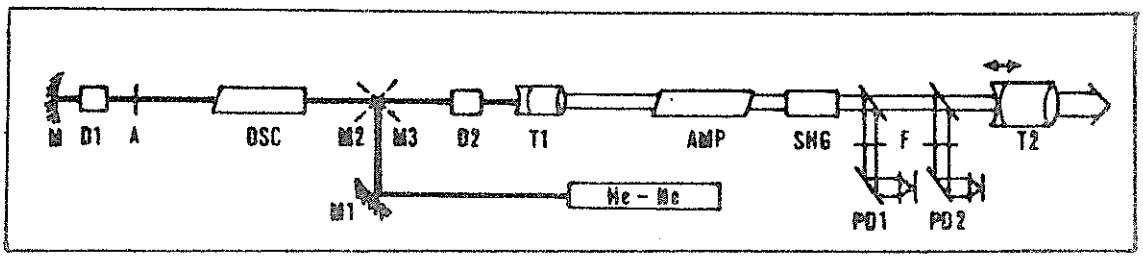

Fig.1. Block diagram of the optical lay-out of the Nd:YAG laser transmitter

M	End mirror	SHG	KDP Frequency doubler
D1	Dye cell	PD1	Monitor detector
A	Aperture	PD2	Start detector
OSC	Oscillator head	F	Neutral density filters
D2	Dye cell	T2	Output telescope
T1	Telescope	M1	Adjustable mirror
AMP	Amplifier head	M2,M3	Removable mirrors

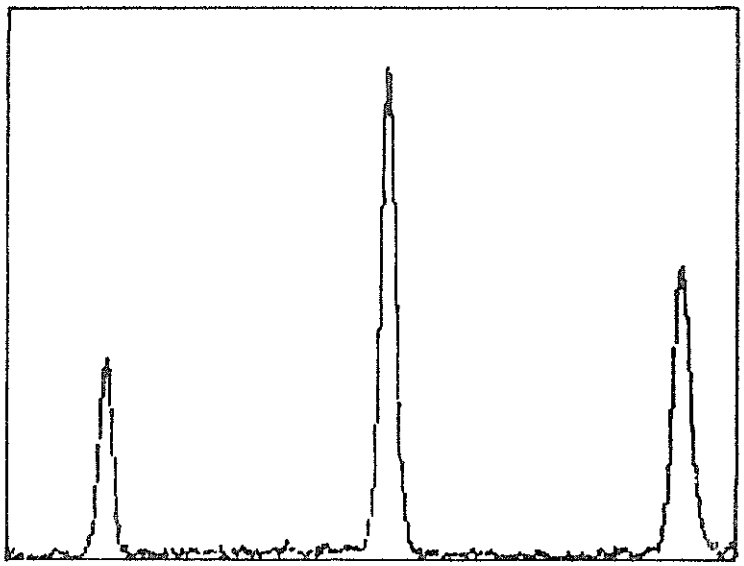

Fig.2. The transmitted pulse
Streak camera trace /5 nsec/screen/

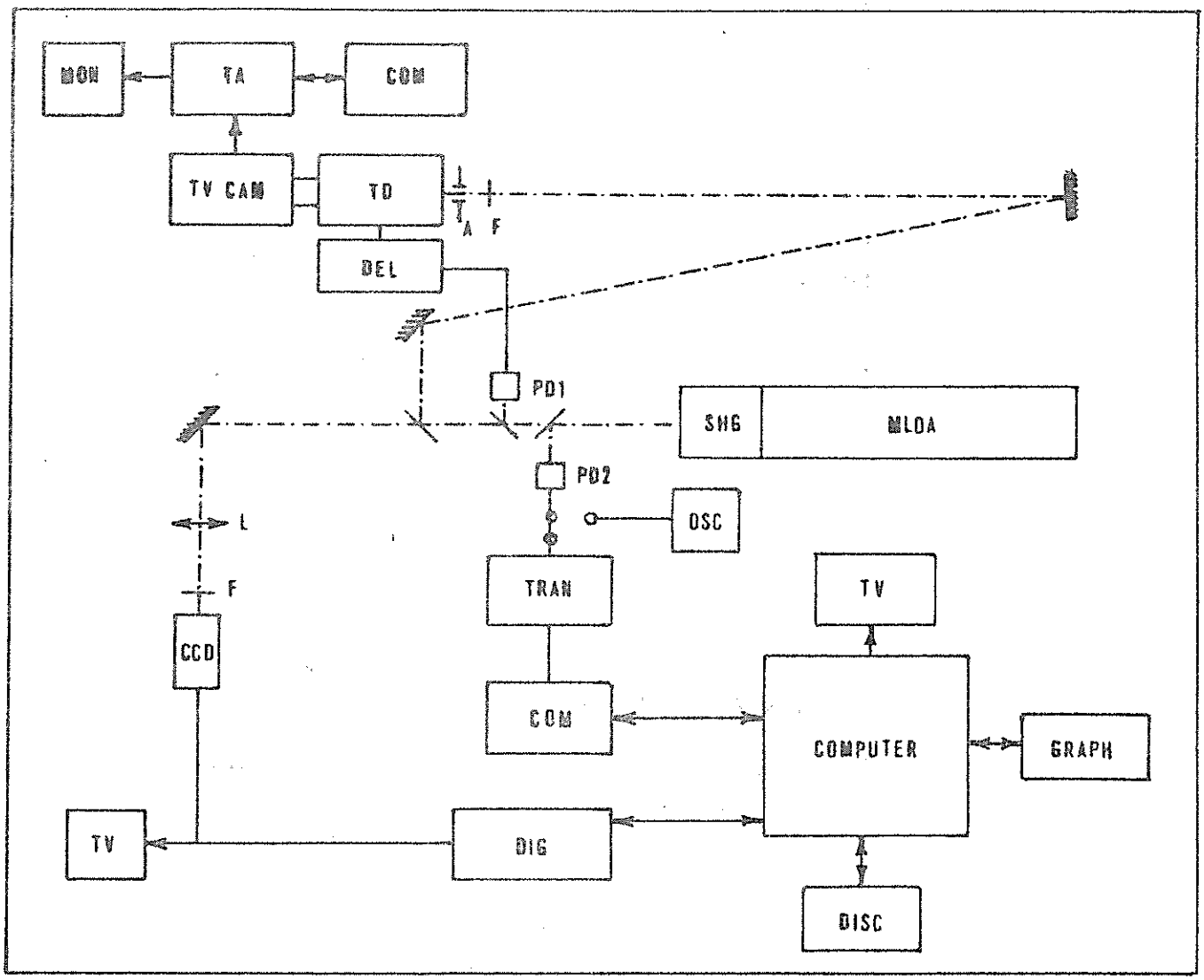

Fig.3. The experimental setup for measuring of the output pulse reproducibility and beam structure

MLOA - Mode locked osc/ampl system, SHG - Frequency doubler, PD1,PD2 - photodiode, TV CAM - SIT TV camera Hamamatsu C1000-12, DEL - Delay unit, TA - Temporal analyzer Hamamatsu C1098, MON - TV monitor, COM - Computer HP 85, F - Neutral density filter, A - Aperture, OSC - Oscilloscope Tektronix 7834, TRAN - Tranzient Digitizer TR 7912A, COMPUTER - HP 21 MX-E, DISC - 50 Mbyte disc, TV - TV monitor, GRAPH - Graphic display, L - Positive lens /f 2.5 m/, CCD - CCD TV camera Fairchild, DIG - Digital Image Memory Quantex, TD - Temporal disperser Hamamatsu C979

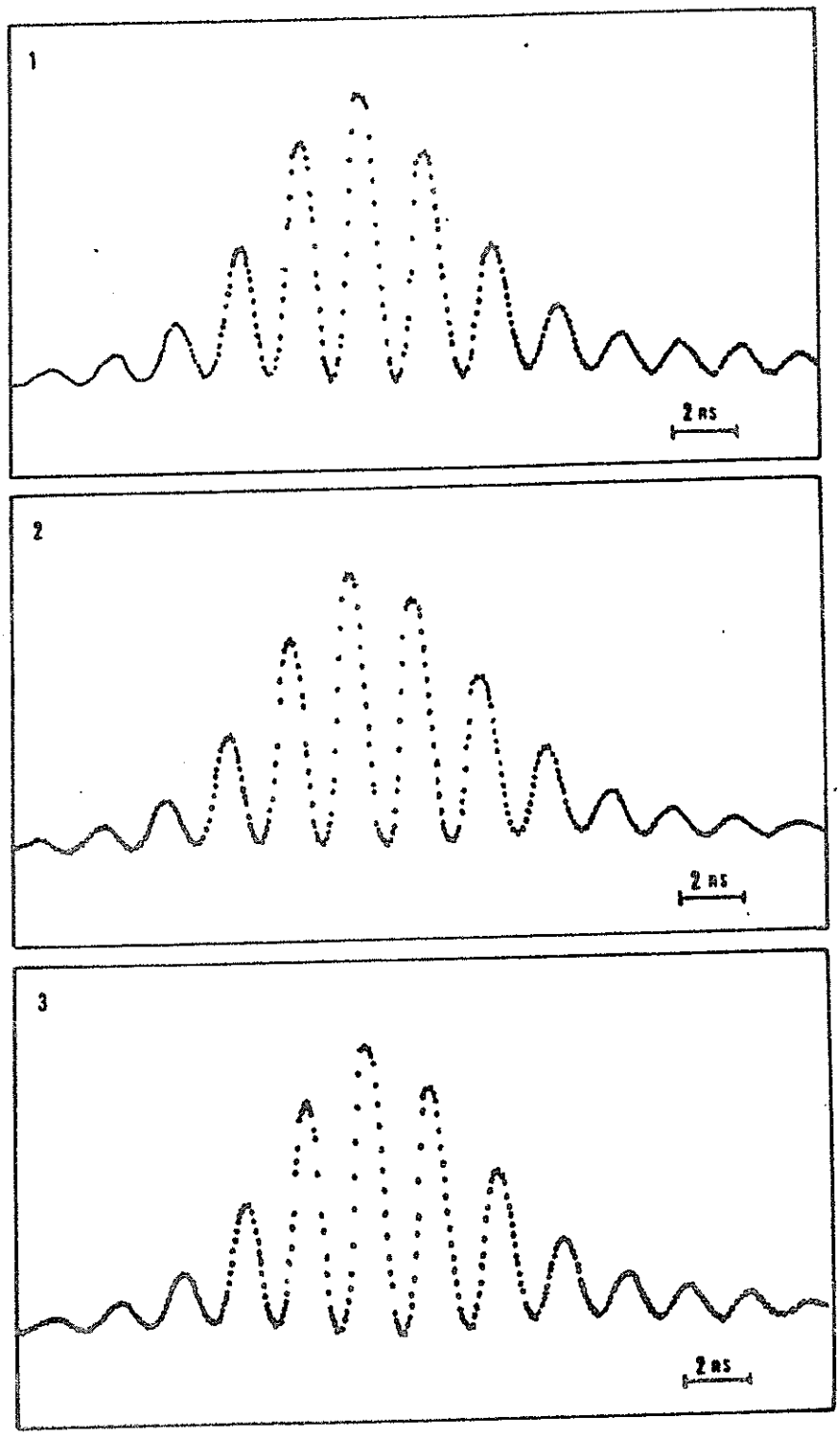

Fig.4. Output ML train long term stability
1 shot No.4000
2 shot No.20000
3 shot No.37000

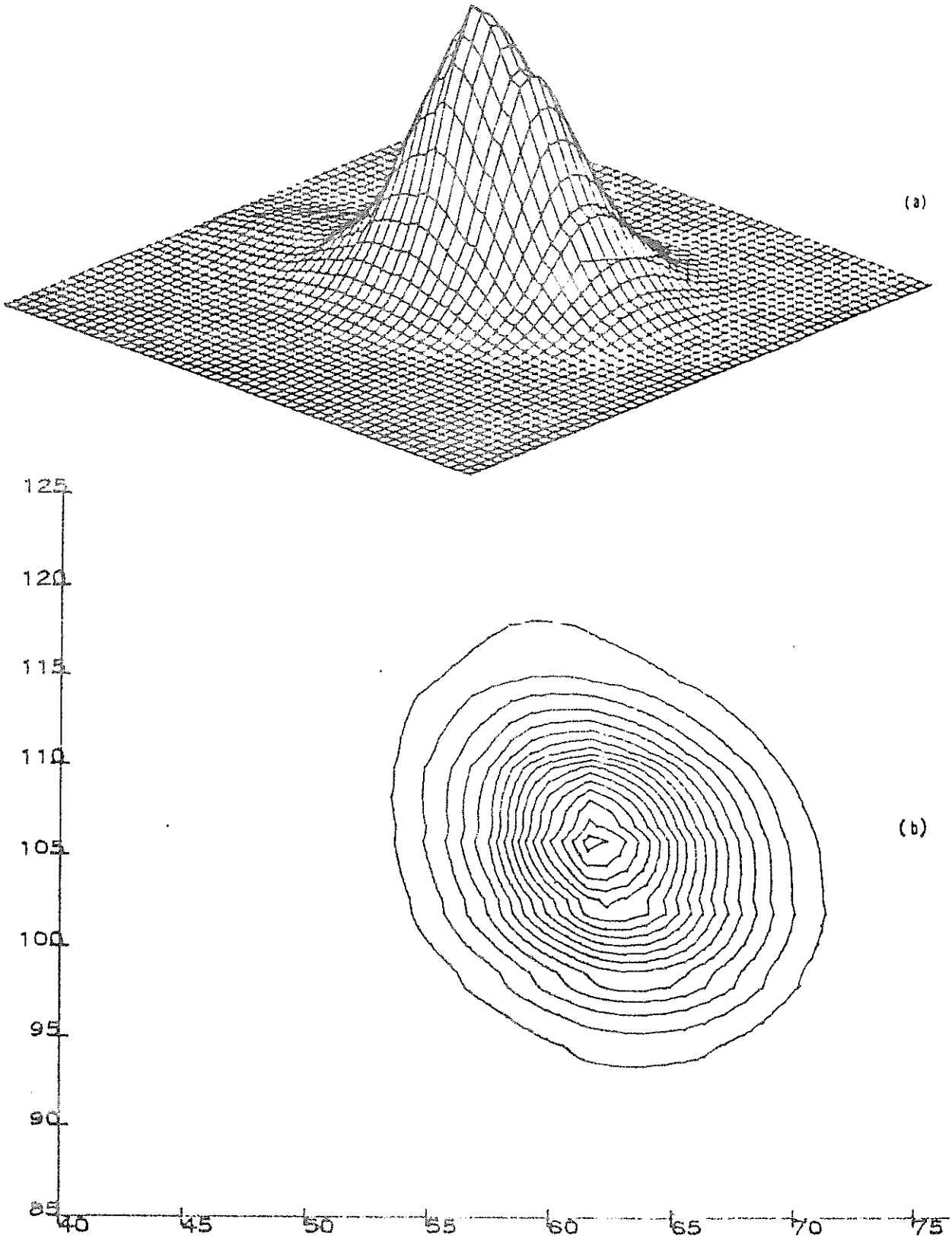

Fig.5. The plot of the 3D projection of the far field beam structure of the oscillator (1.06 μ) (a) the contours (b)

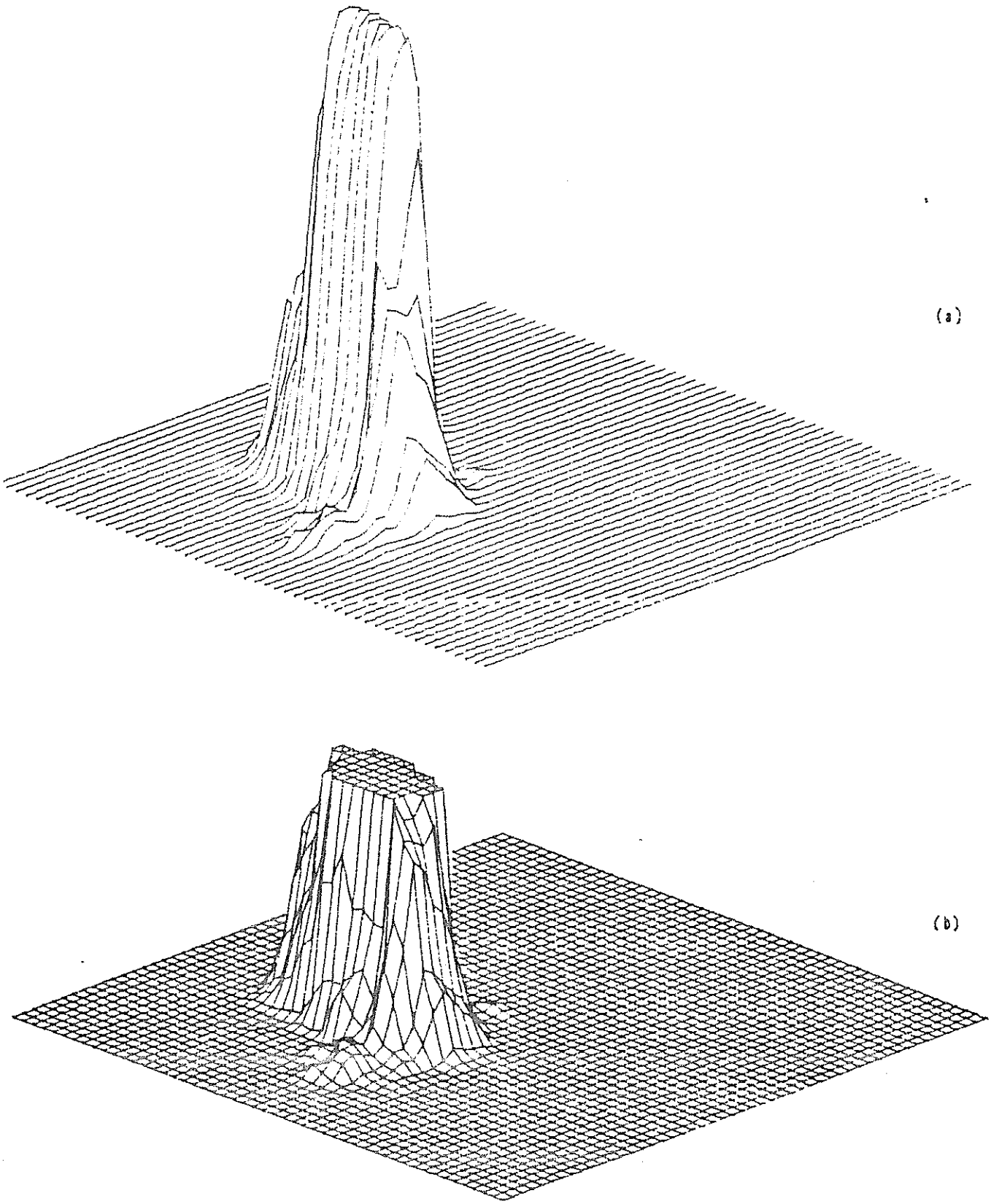

Fig.6. The far field beam structure of the transmitter (osc/ampl/doubler) chain (a) and the half amplitude cut (b)

PRESENT STATUS OF THE CERGA LLR OPERATION

C. Veillet
CERGA
Avenue Nicolas Copernic
06130 Grasse France

Telephone (93) 36 58 49
Telex 470865

ABSTRACT

The CERGA LLR station is now currently operating with a standard range accuracy smaller than 20 cm. The normal points are sent monthly to four scientific teams in France and USA, and are available for the interested people on request to the author.

PRESENT STATUS OF THE CERGA LLR OPERATION

The Figure 1 summarizes the main characteristics of the CERGA LLR operation. The station itself is located in Grasse (south of France) at an elevation of roughly 1300 meters. A 1.5-m reflector is used both for the emission and the reception. The ruby laser has a 3.5 ns pulse and can shoot the Moon every six seconds with a 3 J energy.

The first returns from the Moon have been observed in June 1981, but the first good normal points have been obtained in April 1982, after the solution of some problems with the events timer. Since then,the station has been given normal points (mainly on the Apollo XV reflector) as regularly as possible. The Figure 2 presents an histogram of the number of normal points obtained each month on Apollo XV. The main cause of a lack of results for some months (like February 1984) is the weather linked sometime to a low elevation of the Moon seen from CERGA. In July and August, where the weather is generally good on the French riviera, the nights are very often wet and foggy and the number of results is not as good as it could be expected in such a period.

The Figure 3 shows the distribution of the CERGA normal points with the age of the Moon. At the present time it is possible to obtain data on a reflector illuminated or not, but only during the night or at least after the sunset or before the sunrise. This limitation is not really due to the noise higher during the day than during the night. It is mainly due to the impossibility of pointing the reference craters with the daylight. It should be possible to receive echoes around the full moon. However a lack of results is apparent on the histogram at this phase. These nights have been ruled out from the observation schedule for a long time : the number of observers was not sufficient to cover 20 nights per lunar month. Low moon and bad weather prevented from getting data these last months around the full moon ...

The present laser used at CERGA is an old one. His pulse length prevents to obtain a very good accuracy. A request for money for a new laser and the related equipment will be pre-

sented once more to the french astronomical community in next October. During the waiting of such a change, two improvements are on hand.

The first one concerns the calibration. Made actually on an external target located on a mountain 8 km far from the reflector, it will be obtained as soon as possible on an internal way during the normal laser firings. Thus it will be possible to monitor both the calibration and the pulse length during the observations. The uncertainty on these parameters is the main error source of the CERGA data.

The second improvement concerns the pointing optics (mainly the TV camera) which contrast is too low to permit to point reference craters by daylight. The study of a new system will be made. If its implementation is easy, it would be possible to obtain very soon data in quite all the configurations (night or day on Earth and Moon).

After a reorganization of the LLR team in last November, some modifications have been made concerning the predictions and the analysis of the data. A prediction software has been installed on the main computer of the station. Every observer is thus able to prepare the predictions for the next nights using the last estimates of the Earth rotation parameters. The programm works with an extract of the JPL ephemeris (DE 121 and LLB 13) and gives direct residuals generally lower than 25 ns, giving very rapidly to the observer an insurance on the reality of the echoes.

The normal points are calculated by the LLR team on the CNES computer. It permits quick exchanges inside the station staff and a rapid solution of eventual problems. They are distributed to the interested people as soon as possible after the observations. After some problems of implementation, the software is now working quite well. Dr O. Calame receives directly the data in a file on the CNES computer. JPL and Austin University receive them through Mark III. Everybody else can get the CERGA normal points on request to the author and use them for his scientific work.

A great many people are contributing to the laser station at CERGA beside the author : J.F. Mangin, J.E. Chabaudie, C. Dumoulin, D. Feraudy, J.G. Langlois and J.M. Torre in the LLR team itself. In addition, we wish to thank some other CERGA members who work for one or two nights each month and permit thus to cover more than 20 nights per lunar month.

CERGA LLR

LOCATION

LONGITUDE 43° 45' N

LATITUDE 0h 27m E

ELEVATION 1300 m

1.5-m REFLECTOR for EMISSION and RECEPTION

3.5 nm RUBY LASER - 10 SHOTS PER MINUTE

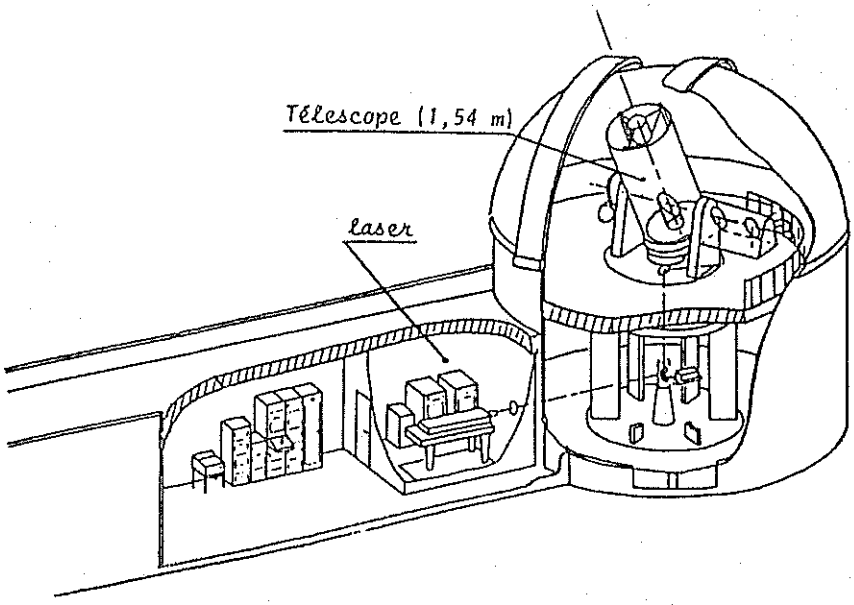

FIGURE 1

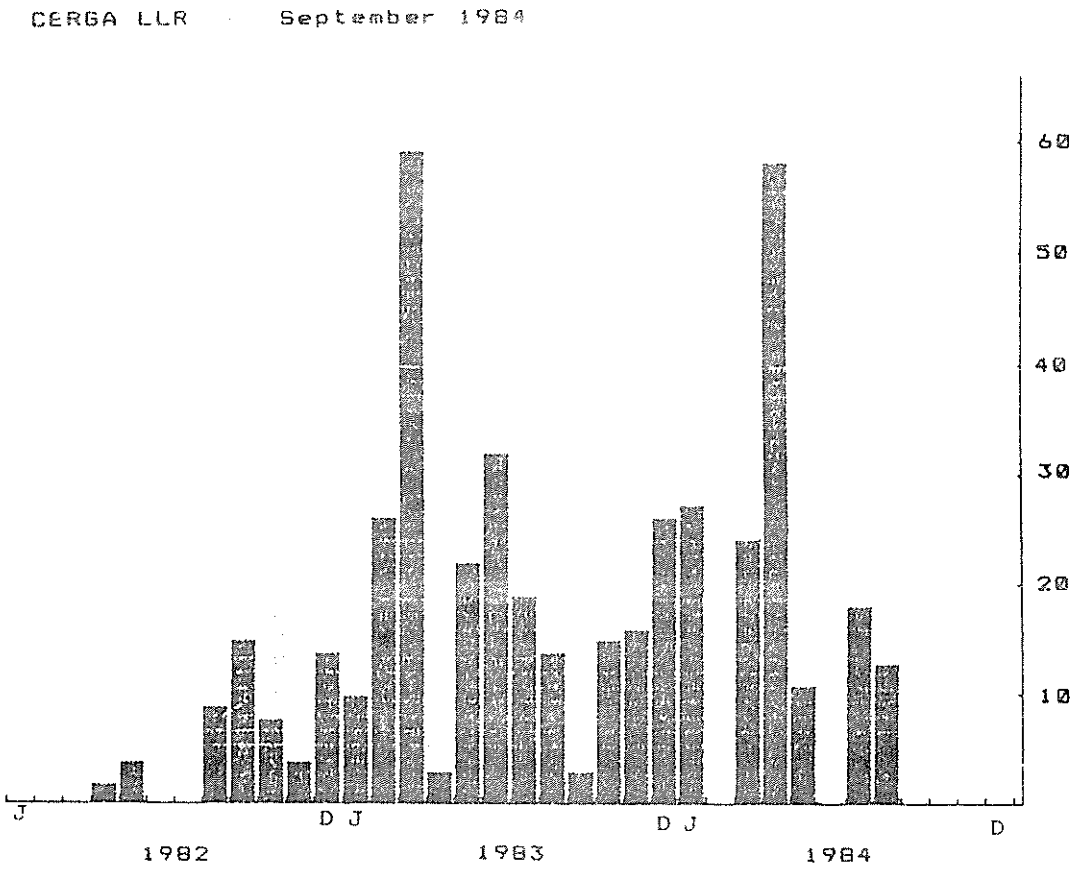

NUMBER OF NORMAL POINTS FOR EACH MONTH (1982-1984)

FIGURE 2

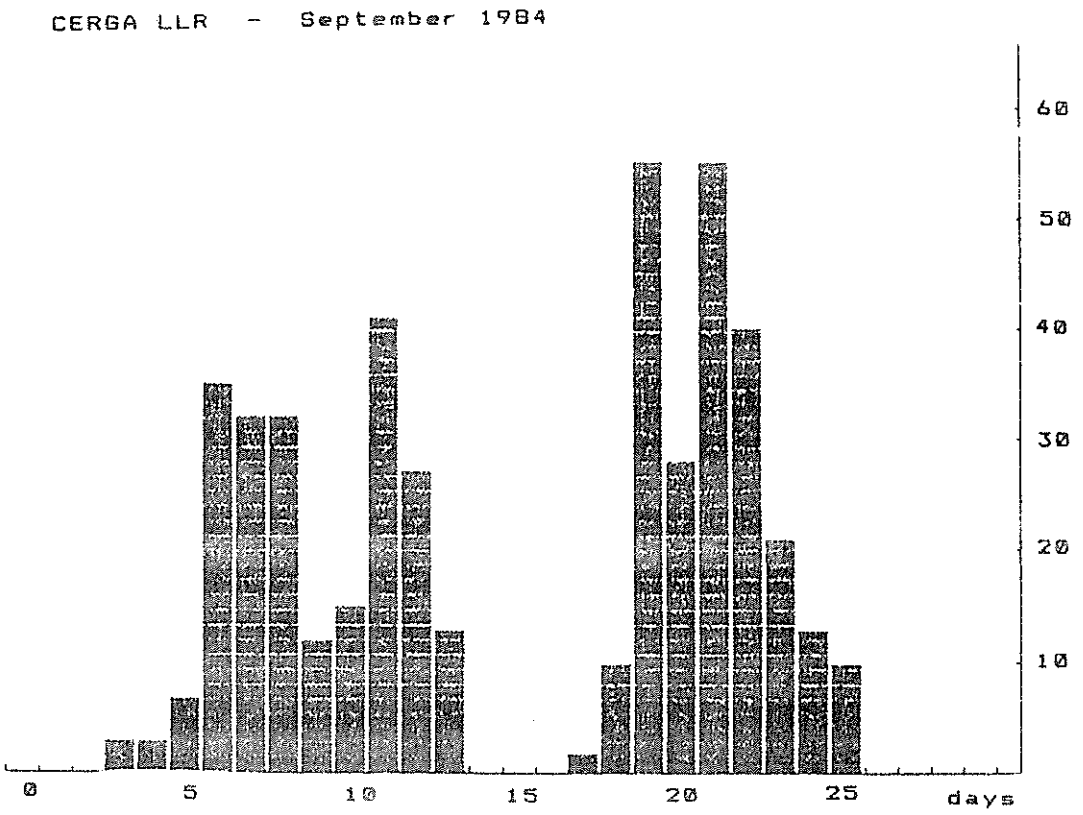

NUMBER OF NORMAL POINTS RELATIVE TO THE AGE OF THE MOON 1982-1984

FIGURE 3

SPECTRAL FILTERS FOR LASER RANGING

B.A. Greene
Division of National Mapping
PO Box 31
Belconnen ACT 2616 Australia

Telephone 062 525095
Telex 62230

H. Visser
Technisch Physische Dienst TNO-TH
Stiettjesweg 1 Delft Posthus 155 Holland

Telephone 78 72 12
Telex 38091

ABSTRACT

The available means of enhancing laser ranging system performance by means of spectral filters are reviewed. Multi-layer dielectric, Fabry -Perot, and Dispersive filters are described, with emphasis on the operational deficiencies and benefits of each filter type. Some projections for the future in spectral filtering for fully optimised system performance are given.

SPECTRAL FILTERS FOR LASER RANGING

1. Introduction

The need for enhancement of signal-to-noise ratio (SNR) in laser ranging systems by means of spectral filtering is continually increasing. For SLR systems the most severe requirements arise for mobile systems which have generally smaller lasers and less well defined coordinates than fixed stations. The combination of poor a priori station coordinates and prediction uncertainties mean that temporal and spatial filtering of the signal is limited, and only spectral filtering can be intensified to enhance SNR.

For LLR systems, it is usual to operate temporal, spatial, and spectral filtering at the design limits of the system, since signal levels are extremely low and noise can be very high (e.g. full moon or daylight ranging).

For laser ranging systems there are two principal parameters which characterise the system performance, signal and SNR. The goal is generally to maximise both, and various measures are taken to accomplish this in terms of varying or modifying system parameters. For example, doubling the laser power doubles signal and SNR, whilst doubling telescope aperture increases signal fourfold whilst not affecting SNR at all.

One of the most cost-effective ways in which most ranging systems can be upgraded is by improving the performance of the spectral filter. Halving the passband of the system spectral filter will double SNR. Doubling the filter throughput efficiency in the passband will double signal. Thus, for example, if an operational system could replace a 1.2A filter of 20% efficiency with a 0.6A filter with 40% efficiency, this would result in a doubling of signal and SNR - the same affect as doubling the laser power, at possibly far less expense.

Considerable emphasis on filter design and selection is also required in the design of minimal, portable, or eye-safe SLR systems.

This paper reviews the filter technology that is available to todays system designers, with the emphasis on operational characteristics. Three basic filter types are reviewed:

(a) Multi-Layer Dielectric Filters (MLDF)

(b) Fabery Perot Filters (FPF)

(c) Dispersion Filters (DF)

2. Multi Layer Dielectric Filters (MLDF)

The principles of operation of MLD filters are well documented in the literature, and widely known. The term MLDF is usually used in the context of laser ranging systems to refer to a composite device consisting of an all-dielectric filter, an induced transmission filter, and a broadband (glass) blocking filter.

The particularly useful features of MLDFs are:

1. Compactness

2. Ruggedness

3. Easy to temperature control or temperature tune

4. Relatively insensitive to incidence angle

5. Single passband only

These features represent why the MLDF is the basic and universal filter for laser ranging systems. It is only in the area of filter efficiency, or transmission, where high performance requirements are difficult to meet with MLDFs. Typical transmission efficiencies for fully blocked filters range from 60% at 10A bandwidth to 20% at 1A. Other filter types become superior in transmission for filter bandwidths below about 3A.

For filter bandwidths in excess of 3A, efficiencies of 50% (and higher) can be obtained for MLDFs. This value of throughput, together with the advantages listed above, make them the natural first choice for most laser ranging systems.

3. Fabery Perot Filters

MLDFs evolved several decades ago from classical Fabery perot filters (FPF). The family similarities remain in that both use interferometric principles to enhance or retard transmission. FPFs, however, use two mirrors separated by a distance which is very large compared to the wavelength of light, and for some applications this original configuration can be utilised to better effect than the MLDF.

In particular, high transmission efficiencies coupled with very narrow bandwidths may be realised. For example, a blocked FPF with 0.5A bandwidth may have 40-60% transmission at line centre - approximately double that realisable with an equivalent bandwidth MLDF. At first sight this looks extremely attractive, but there are many factors weighing against the operational application of FPFs.

The principal difficulties with FPFs arise in the following areas:

(a) Free Spectral Range (FSR) and blocking

(b) Bandwidth control

(c) Angular sensitivity

(d) Vibration sensitivity

(e) Temperature sensitivity

(f) Field-of-view (FOV) problems

(g) Alignment/Servo is highly specified

The Free Spectral Range (FSR) is the distance from one peak of transmission to another in the 'comb' response of the FPF. It is given by

$$FSR = \lambda^2/2d$$

where λ = centre (design) wavelength

d = plate separation

The finesse (F) of the filter is made up of a number of terms, but in practice is usually given by

$$F = \pi R^{\frac{1}{2}} /(1-R)$$

where R = reflectivity of FP mirrors

Bandwidth (BW) is given by

$$BW = FSR/F$$

If (typically) $\lambda = 532$ nm

$d = 0.1$ mm

$F = 28$

then $FSR = 14A$

$BW = 0.5A$

This represents a typical FPF design.

Now the overall efficiency of the FPF itself may be as high as 85% if the device is very precisely manufactured and aligned. However, because the passband recurs at a frequency given by the FSR, a blocking filter must be used to eliminate all but the desired passband. The blocking filter passband must be less than the FSR to avoid passing more than one passband. In the above example, a 10A MLD filter would be used, yielding an overall efficiency of around 50%.

FPFs are extremely sensitive to angle detuning, because the interferometric operation depends upon the path length travelled between mirrors to be an integral number of half wavelengths. It is simple to establish the angle sensitivity as

$$\Delta\lambda = \lambda_c \left(\frac{1}{\cos\theta} - 1\right)$$

or

$$\theta = \cos^{-1}\left(\lambda_c/(\lambda_c + \Delta\lambda)\right)$$

for $\lambda = 5320$ A

$\Delta\lambda = 0.1$ A

then $\theta = 1264$ arc sec.

If the filter is working at a X60 demagnification from the receiving telescope, then the centre wavelength of the filter will move 0.1A over a 21 arc second field of view. More significantly, the filter must be held stable to 21 arc minutes (1264 secs) in its holder if the centre frequency is not to move by more than 0.1A.

It is important to note also that spatial filtering must complement the FPF, since the filter only 'works' at normal incidence, and the passband simply moves (spectrally) with angle of incidence. That is, the system FOV is dictated by the FPF design.

Temperature effects can be the limiting factor in FPF implementation. Even INVAR stabilised mounts can 'walk' a filter line centre by up to 3A per °C. For a 0.5A filter, 0.5°C temperature control is totally unsatisfactory.

A recent development has been the active control, using PZT or similar drive, of the parallelism and spacing of the FP mirrors. Using a CW laser injected off-axis and directed to a detector, the FP tilt and spacing can be servo controlled for optimum performance. The off-axis alignment laser can be at any wavelength, but is often at 6328A as little power is required. A dither technique is used to lock the FPF to line centre of this laser, and the on-axis passband tuned to the desired wavelength by tuning the incidence angle of the alignment laser. This technique has been very successful in overcoming mount creep, temperature drift, and even some vibration-induced detuning of the FPF in tests at the Orroral Observatory. However, the hardware is complex and sensitive, and major efficiency improvements over MLDFs must be demonstrated before the major task of integrating FPFs should be undertaken.

The Orroral Observatory is extending its examination of FPF characteristics to determine the realisable peak transmission efficiency, the long term stability, and the (light) noise immunity of FPF servo systems.

4. Dispersive Filters

Both refraction and diffraction can be used as the dispersive mechanism for dispersive filters. Refractive-Dispersive Filters (RDFs) and Diffractive-Dispersive Filters (DDFs) are both common in a wide range of optical applications. It is only recently [1] that either has been used for laser ranging.

The principal of operation of these devices is extremely simple. The spectral dispersion of the incident radiation allows spatial isolation of narrow wavebands of interest by means of spatial filtering (pinholes, slits).

The significant features of DFs in general can be summarised as:

(a) temperature stable

(b) vibration/mechanical noise sensitive

(c) complex design and optical fabrication

(d) relatively high efficiencies possible

(e) widely and easily tuneable

(f) efficiency not bandwidth dependent

(g) bandwidth also tuneable

(h) bandwidth and field of view not independently adjustable

(i) precision alignment necessary

Apart from these general characteristics, each type of DF has specific advantages and disadvantages. DDFs have an unfortunate characteristic which causes temporal dispersion of the processed optical signal. Precision correction for this effect, due to the non-normal incidence of the input beam on the grating, is extremely difficult. Thus an additional ranging error is introduced. Further, the dispersive mechanism is not more efficient than 50-60%. Finally the coupling of bandwidth and FOV by the exit slit (spatial filter) results in impractically small FOV for very narrow bandwidths. A typical DDF [1] will give 3.5A per 60 arc sec FOV. Thus a 0.5A exit slit would give a maximum FOV of 9 arc seconds. Increasing the FOV is not possible without expanding the BW also, despite the fact that this is detrimental to system performance. The example given will give a BW of 2A for a FOV of 35 arc seconds and an efficiency of 50%, a performance level around which an excellent SLR may be built.

RDF characteristics do not include temporal dispersion of the signal, and efficiencies near 90% are feasible. The major limitation with RDF application is the practical limit to the size of dispersive prisms which can be constructed. This limits the degree of dispersion attainable, and filters for (typical) ranging configurations may be limited to 3A (min) by

this. However, it is unlikely that an RDF of less than 3A would be of general use, since the FOV for smaller bandwidths becomes unreasonably small.

5. Future Developments

Further development is likely to see incremental improvements in MLDF efficiency at all bandwidths.

The use of FPF technology should move gradually into the operational sector from the research environment.

A most promising long term development is the combination of FPF and DDF to form 0.5A filters with 75% throughput in the centre of the passband. This proposed design would use the DDF in its optimum role - as a high efficiency wide band filter. Thus the DDF would not limit the system FOV. If a DDF was used as (say) a 10A block for a 0.5A FPF with 14A free spectral range, an efficiency of 90% is possible, with a working FOV of an arc minute. This FOV can then be controlled independently of the spectral filtering process using a conventional lens/pinhole combination. This is not really necessary, since in the DDF/FPF combination, the DDF can be used as the spatial filter as its transmission efficiency will not vary as its FOV and bandwidth are tuned. Clearly a FOV corresponding to a DDF bandwidth greater than 14A cannot be selected, since the DDF is then not effectively blocking the FPF. Similarly, a FOV corresponding to a DDF bandwidth of less than 0.5A cannot be selected without reducing the effective bandwidth of the DDF/FPF combination. This lower limit of filter bandwidth is most likely to be fixed by the power spectrum of the laser. For a 100 ps laser, a filter of around 0.6A is needed to transmit the power spectrum. If a 0.6A FWHM filter is used, a large proportion of the signal from a 100 ps laser will be transmitted at an efficiency below the peak transmission of the filter.

For the example given above, if a FPF efficiency of 85% can be achieved routinely, then the spectral filter will operate at 75% efficiency for 0.5A bandwidth over a wide range of FOV. This is four times better than MLDF performance, and almost 1.5 times as good (efficient) as a MLDF blocked FPF.

Large systems, and particularly LLR systems will gain 300% to 50% improvements in data production over current capabilities at 0.5A.

EPOCH TIMING FOR LASER RANGING

B.A. Greene
Division of National Mapping
PO Box 31
Belconnen ACT 2616 Australia

Telephone 062 525095
Telex 62230

ABSTRACT

The well established advantages of epoch timing are reviewed in the light of recent and iminent developments in laser ranging hardware. The capability of asymetric Stop-Start time interval measurement techniques to meet the emerging demands for timing system precision, accuracy, and event rates is questioned. The ability of systems using epoch timing to adapt to the new technology and meet the highest performance specifications is emphasised.

EPOCH TIMING FOR LASER RANGING

1. Introduction

The advantages of epoch timing for laser ranging have been known for some time. Some of the earliest timing equipment specifically designed for laser ranging used epoch timing principles (e.g. the 'Maryland' event timer).

The principal advantages of epoch timing have been:

1. Measurement symmetry for START and STOP.

2. Capability to accommodate many shots in flight with a single instrument (i.e. multiple-stop capability).

3. Precise epochs are produced as well as range measurements.

Recent developments have highlighted these advantages as well as throwing light on some previously undetected advantages.

2. Epoch Timing Principles

A epoch timing system measures range by determining the epoch of the transmission and reception of the laser pulse, and obtaining the difference by subtraction.

An epoch timing system can be constructed from commercial electronics modules, since all that is required is a scaler/counter and a time interval unit (TIU). If the scaler and TIU are properly chosen, the epoch precision is the precision of the TIU. The specification for these 2 components are that the maximum count of the TIU must be greater than the period (1/f) at which the scaler is clocked. The scaler is simply latched by the event, which also starts the TIU, which is stopped by the same clock pulse which clocks (increments) the scaler. For example, the original (1974) Orroral LLR timing system consisted of a 10 MHz scaler, which, when latched, gave 100 ns precision epoch. The event which latched the scaler also started the 1ns precision TIU, which was stopped by a 100 KHz pulse train, giving a maximum count of 10 microseconds.

The epoch is given by

$$E = L + (c - t)$$

where L = epoch latched in scaler
c = maximum count of TIU
t = TIU measurement

In practice the epoch E is formed in a minicomputer which first truncates L to eliminate least significant digits which would overlap (c-t). If the STOP pulse train going to the TIU is not in phase with the latch clock pulse to better than the precision of the TIU, then additional adjustments need to be made to E.

The epoch E will be absolutely accurate only to the extent that the frequency standard which supplies the latch clock/TIU stop is absolutely accurate. If the clock rate is known, then the epoch accuracy can be upgraded in post-processing. The range measurements derived from these epochs will have a precision approximately equal to 1.4 times the epoch precision plus the frequency standard's error over the measurement interval.

The major difficulties in epoch timing systems are:

1. Overlapping of START and STOP events in TIU.

2. Perfect recombination of E and (c-t) to give precise epoch.

The overlapping of START and STOP events in the TIU will generally cause errors. Some systems employ two TIUs with one TIU having its STOP channel input frequency 180 degrees out of phase with the other, so that overlap can be avoided. This of course introduces more calibration complexity, but has been successful. An alternative is to make the TIU input pulses very short, and the maximum count very long, and accept overlaps. For example if the pulses were 4 ns wide and the max count 1000 ns, only 0.4% of measurements would be affected. Lengthening the max count also makes combining the TIU and scaler readings simpler, as more overlapping digits occur for longer counts, and the software algorithm for combining the two numbers into a single epoch is simpler.

3. Recent Developments

Laser ranging systems now routinely operate with a single-shot precision of 5 cm. Soon 2 cm single-shot precisions will be routine, based on new laser, receiver, and timing system technology. The precisions required by the new laser ranging systems may demand the adoption of epoch timing techniques.

An acceptable standard for ranging timing systems for the next 5 years is likely to be 30 ps (RMS) accuracy in range over 100 ms ranges, and 50 ps over lunar ranges. It is now relatively easy to acquire or even construct a TIU with 20-30 ps precision. However very few available designs will maintain this precision over more than a few microseconds. One exception, the HP5370 series TIU, limits the rate at which the laser can be fired to 5 Hz once the max count exceeds 50 ms.

Thus the newer technology in TIUs may be applicable only as the vernier, or as an add-on, to an existing measurement system. Since epoch timing scalers can easily run up to 100 MHz, giving a TIU max count requirement of 10 ns, minimal demands are placed on the TIU in this regard by epoch timing. That is, epoch timing systems are ideally suited to take advantage of high precision, short count TIUs.

An additional problem for conventional systems using direct time interval measurements to measure range arises from temperature drift of TIUs. It has recently been discovered that the HP5370B shows a measurement bias of 10 ps per degree Celsius. Other TIUs show similar biases. The error, which is systematic, does not depend on the length of count, and thus is removed entirely if the TIU is used as the vernier for an epoch timing system, since the error will occur in both epochs, and cancel out in the formulation of a time interval by subtraction.

The development of solid-state pumping for Nd:YAG lasers raises the possibility of significant improvements in laser efficiency, and may lead to higher repetition rate capabilities well beyond the present 10 Hz. At 200 Hz repetition rates, even the lower satellites will require multiple shots in flight. If recent developments in detector technology lead to 1 micron ranging systems, even higher rates could be required. Only epoch timing techniques can meet these event rate specifications. (The data acquisition and control specification is not considered here.)

Finally, new streak cameras are now available which allow 2-D scanning of the electron beam. If such a streak tube was to be integrated with a 2-D CCD array of large dimensions, then it is conceivable that it could be used as a picosecond precision vernier for an epoch timing system. If the 2-D scanning algorithm is correctly specified, it is possible to use a large proportion of the addressable space on the CCD to give an unambiguous, picosecond precision epoch readout over long periods (up to 10 ns, i.e. 10 ns maximum count). It seems unlikely that this ultra-high precision development will integrate naturally with timing systems other than epoch timing systems.